

Atomic
and
nuclear physics

P6 Atomic and nuclear physics

P 6.1 Introductory experiments

P 6.1.1	Oil-spot experiment	205
P 6.1.2	Millikan experiment	206
P 6.1.3	Specific electron charge	207
P 6.1.4	Planck's constant	208–209
P 6.1.5	Dualism of wave and particle	210
P 6.1.6	Paul trap	211

P 6.2 Atomic shell

P 6.2.1	The Balmer series of hydrogen	212
P 6.2.2	Emission and absorption spectra	213
P 6.2.3	Inelastic electron collisions	214
P 6.2.4	Franck-Hertz experiment	215–216
P 6.2.5	Critical potential	217
P 6.2.6	Electron spin resonance (ESR)	218
P 6.2.7	Normal Zeeman effect	219
P 6.2.8	Optical pumping (anomalous Zeeman effect)	220

P 6.3 X-rays

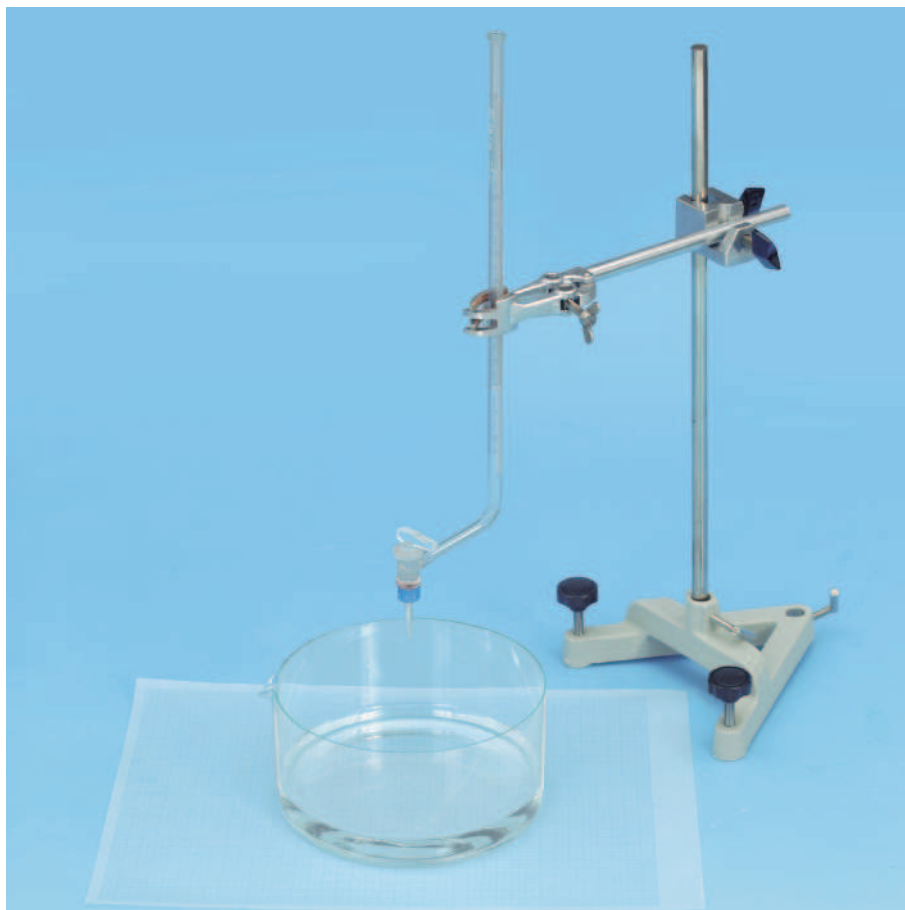
P 6.3.1	Demonstrating x-rays	221
P 6.3.2	Attenuation of x-rays	222
P 6.3.3	Physics of the atomic shell	223
P 6.3.4	X-ray physics with the x-ray apparatus P	224

P 6.4 Radioactivity

P 6.4.1	Detection of radioactivity	225
P 6.4.2	Poisson distribution	226
P 6.4.3	Radioactive decay and half-life	227
P 6.4.4	Attenuation of α , β and γ radiation	228

P 6.5 Nuclear physics

P 6.5.1	Demonstration of particle tracks	229
P 6.5.2	Rutherford scattering	230
P 6.5.3	Nuclear magnetic resonance (NMR)	231
P 6.5.4	α spectroscopy	232
P 6.5.5	γ spectroscopy	233
P 6.5.6	Compton effect	234



Determining the size of oil molecules (P 6.1.1.1)

P 6.1.1**Oil-spot experiment**

P 6.1.1.1 Determining the size of oil molecules

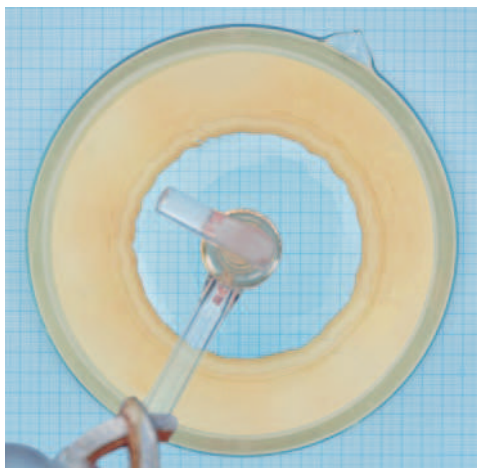
Cat. No.	Description	P 6.1.1.1
664 179	Crystallization dish, 230 mm dia., 100 mm high	1
665 844	Burette, 10 ml: 0.05, w. lateral stopcock, amber glass, Schellbach blue line	1
664 110	Beaker, 50 ml, ss, hard glass	1
665 751	Graduated cylinder, 10 ml: 0.2	1
665 754	Graduated cylinder, 100 ml: 1	1
300 02	Stand base, V-shape, 20 cm	1
300 43	Stand rod, 75 cm	1
301 01	Leybold multiclamp	1
666 555	Universal clamp, 0...80 mm	1
675 3410	Water, pure, 5 l	1
672 1240	Glycerin trioleate, 100 ml	1
674 2220	Benzine, 40–70°C	1
670 6920	Lycopodium spores, 25 g	1

One important issue in atomic physics is the size of the atom. An investigation of the size of molecules makes it easier to come to a usable order of magnitude by experimental means. This is estimated from the size of an oil spot on the surface of water using simple means.

In this experiment, a drop of glycerin nitrioleate as added to a grease-free water surface dusted with *Lycopodium* spores. Assuming that the resulting oil spot has a thickness of one molecule, we can calculate the size d of the molecule according to

$$d = \frac{V}{A}$$

from the volume V of the oil droplet and the area A of the oil spot. The volume of the oil spot is determined from the number of drops needed to fill a volume of 1 cm^3 . The area of the oil spot is determined using graph paper.

Determining the area A of the oil spot

P 6.1.2

Millikan experiment

- P 6.1.2.1 Determining the electrical charge of the electron after Millikan and demonstrating the quantum nature of the charge – measuring the suspension voltage and the falling speed
- P 6.1.2.2 Determining the electrical charge of the electron after Millikan and demonstrating the quantum nature of the charge – measuring the rising speed and the falling speed
- P 6.1.2.3 **CASSY-S** Determining the electrical charge of the electron after Millikan and demonstrating the quantum nature of the charge – measuring the suspension voltage and the falling speed with CASSY
- P 6.1.2.4 **CASSY-S** Determining the electrical charge of the electron after Millikan and demonstrating the quantum nature of the charge – measuring the rising speed and the falling speed with CASSY



Determining the electrical charge of the electron after Millikan and demonstrating the quantum nature of the charge – measuring the suspension voltage and the falling speed (P 6.1.2.1)

With his famous oil-drop method, *R. A. Millikan* succeeded in demonstrating the quantum nature of minute amounts of electricity in 1910. He caused charged oil droplets to be suspended in the vertical electric field of a plate capacitor and, on the basis of the radius r and the electric field E , determined the charge q of a suspended droplet:

$$q = \frac{4\pi}{3} \cdot r^3 \cdot \frac{\rho \cdot g}{E}$$

ρ : density of oil
 g : gravitational acceleration

He discovered that q only occurs as a whole multiple of an electron charge e .

His experiments are produced here in two variations. In the first variation, the electric field

$$E = \frac{U}{d}$$

d : plate spacing

is calculated from the voltage U at the plate capacitor at which the observed oil droplet just begins to hover. The constant falling velocity v_1 of the droplet when the electric field is switched off is subsequently measured to determine the radius. From the equilibrium between the force of gravity and Stokes friction, we derive the equation

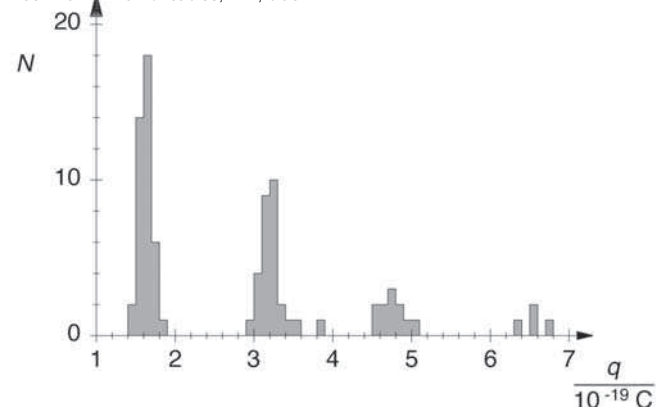
$$\frac{4\pi}{3} \cdot r^3 \cdot \rho \cdot g = 6\pi \cdot r \cdot \eta \cdot v_1$$

η : viscosity

In the second variant, the oil droplets are observed which are not precisely suspended, but which rise with a low velocity v_2 . The following applies for these droplets:

$$q \cdot \frac{U}{d} = \frac{4\pi}{3} r^3 \cdot \rho \cdot g + 6\pi \cdot r \cdot \eta \cdot v_2$$

Cat. No.	Description	P 6.1.2.1	P 6.1.2.2	P 6.1.2.3	P 6.1.2.4
559 411	Millikan apparatus	1	1	1	1
559 421	Power supply for Millikan apparatus	1	1	1	1
313 033	Electronic stopclock P	1	2		
524 010USB	Sensor-CASSY			1	1
524 200	CASSY Lab			1	1
524 034	Timer box			1	1
501 46	Pair of cables, 1 m, red and blue	3	4	3	3
500 421	Connecting lead, 50 cm, red				1
additionally required:					
PC with Windows 95/98/NT or higher					
501 461	Pair of cables, 1 m, black			1	1



The histogram reveals the quantum nature of the charge

Additionally, the falling speed v_1 is measured, as in the first variant. The measuring accuracy for the charge q can be increased by causing the oil droplet under study to rise and fall over a given distance several times in succession and measuring the total rise and fall times.



Determining the specific charge of the electron (P 6.1.3.1)

P 6.1.3**Specific electron charge****P 6.1.3.1** Determining the specific charge of the electron

Cat. No.	Description	P 6.1.3.1
555 571	Fine beam tube	1
555 581	Helmholtz coils with holder and measuring device	1
521 65	DC power supply 0...500 V	1
521 545	DC power supply 0...16 V, 5 A	1
531 120	Voltmeter, DC, $U \leq 300$ V, e. g. Multimeter LD analog 20	1
531 120	Ammeter, DC, $I \leq 3$ A, e. g. Multimeter LD analog 20	1
531 835	Universal Measuring Instrument Physics	1*
524 0382	Axial B-Sensor S	1*
501 11	Extension cable, 15-pole	1*
311 77	Steel tape measure, 2m	1
500 614	Safety connection lead, 25 cm, black	3
500 624	Safety connection lead, 50 cm, black	3
500 644	Safety connection lead, 100 cm, black	7

* additionally recommended

The mass m_e of the electron is extremely difficult to determine in an experiment. It is much easier to determine the specific charge of the electron

$$\varepsilon = \frac{e}{m_e}$$

from which we can calculate the mass m_e for a given electron charge e .

In this experiment, a tightly bundled electron beam is diverted into a closed circular path using a homogeneous magnetic field in order to determine the specific electron charge. The magnetic field B which diverts the electrons into the path with the given radius r is determined as a function of the acceleration voltage U . The Lorentz force caused by the magnetic field acts as a centripetal force. It depends on the velocity of the electrons, which in turn is determined by the acceleration voltage. The specific electron charge can thus be determined from the measurement quantities U , B and r according to the formula

$$\frac{e}{m_e} = 2 \cdot \frac{U}{B^2 \cdot r^2}$$



Circular electron path in fine beam tube

P 6.1.4**Planck's constant**

- P 6.1.4.1 Determining Planck's constant – measuring with a compact assembly
- P 6.1.4.2 Determining Planck's constant – dispersion of wavelengths with a direct-vision prism on the optical bench



Determining Planck's constant – measuring with a compact assembly (P 6.1.4.1)

Cat. No.	Description	P 6.1.4.1	P 6.1.4.2
558 77	Photo cell for determining Planck's constant	1	1
558 79	Compact arrangement for determining Planck's constant	1	
558 791	Supply unit for photo cell		1
451 15	High-pressure mercury lamp	1	1
451 19	Lamp socket E27 on rod for high-pressure mercury lamp		1
460 373	Optics rider, H = 60 mm/W = 50 mm		1
460 380	Cantilever arm		1

When light with the frequency ν falls on the cathode of a photo-cell, electrons are released. Some of the electrons reach the anode where they generate a current in the external circuit, which is compensated to zero by applying a voltage with opposite sign $U = -U_0$. The applicable relationship

$$e \cdot U_0 = h \cdot \nu - W, \quad W: \text{electronic work function}$$

was first used by *R. A. Millikan* to determine Planck's constant h .

In the first experiment, a compact arrangement is used to determine h , in which the light from a high-pressure mercury vapor lamp is spectrally dispersed in a direct-vision prism. The light of precisely one spectral line at a time falls on the cathode. A capacitor is connected between the cathode and the anode of the photocell which is charged by the anode current, thus generating the opposing voltage U . As soon as the opposing voltage reaches the value $-U_0$, the anode current is zero and the charging of the capacitor is finished. U_0 is measured without applying a current by means of an electrometer amplifier.

The second experiment uses an open arrangement on the optical bench. Here as well, the wavelengths of the light are dispersed using a direct-vision prism. The opposing voltage U is tapped from a DC voltage source via a voltage divider, and varied until the anode current is compensated precisely to zero. The I-measuring amplifier D is used for conducting sensitive measurements of the anode current.

Cat. No.	Description	P 6.1.4.1	P 6.1.4.2
451 30	Universal choke 230 V, 50 Hz	1	1
532 14	Electrometer amplifier	1	
562 791	Plug-in unit 230V/12 V AC/20 W; with female plug	1	
532 00	I-measuring amplifier D		1
531 120	Multimeter LDanalog 20	1	2
575 24	Screened cable BNC/4 mm	1	
576 74	Rastered socket panel, DIN A4		1
576 86	STE mono cell holder		2
577 93	STE 10-turn potentiometer 1 k Ω , 2 W		1
578 22	STE capacitor 100 pF, 630 V	1	
579 10	STE key switch (n.o.), single-pole	1	
501 48	Set of 10 bridging plugs		1
503 11	Set of 20 batteries 1.5 V (type MONO)		1
460 32	Precision optical bench, standardized cross section, 1 m		1
460 34	Auxiliary bench w. swivel joint, protractor and index bench, 0.5 m		1
460 374	Optics rider, H = 90 mm/W = 50 mm		1
460 375	Optics rider, H = 120 mm/W = 50 mm		5
460 02	Lens f = + 50 mm		1
460 08	Lens f = + 150 mm		1
460 14	Adjustable slit		1
460 13	Projection objective, f = + 150 mm		1
466 05	Direct-vision prism		1
466 04	Holder for direct-vision prism		1
502 04	Distribution box	1	
590 011	Clamping plug	2	
500 414	Connection lead, black, 25 cm	1	
500 440	Connection lead, yellow-green, 100 cm	1	
500 444	Connection lead, black, 100 cm		1
501 45	Pair of cables, 50 cm, red and blue	1	2
501 461	Pair of cables, 1 m, black	1	
463 51	Diaphragm with 5 slits		1
577 40	STE resistor 470 Ohm, 1.4 W		1

**P 6.1.4****Planck's constant**

P 6.1.4.3 Determining Planck's constant – selection of wavelengths with interference filters on the optical bench

Determining Planck's constant – selection of wavelengths with interference filters on the optical bench (P 6.1.4.3a)

Cat. No.	Description	P 6.1.4.3 (a)	P 6.1.4.3 (b)
558 77	Photo cell for determining Planck's constant	1	1
558 791	Holder for photo cell	1	1
451 15	High-pressure mercury lamp	1	1
451 19	Lamp socket E27 on rod for high-pressure mercury lamp	1	1
460 03	Lens $f = +100$ mm	1	1
460 26	Iris diaphragm	1	1
558 792	Filter wheel with iris diaphragm	1	1
468 401	Interference filter 578 nm	1	1
468 402	Interference filter 546 nm	1	1
468 403	Interference filter 436 nm	1	1
468 404	Interference filter 405 nm	1	1
451 30	Universal choke 230 V, 50 Hz	1	1
532 14	Electrometer amplifier	1	1
562 791	Plug-in unit 230V/12 V AC/20 W; with female plug	1	1
578 22	STE capacitor 100 pF, 630 V	1	1
579 10	STE key switch n.o. single-pole	1	1
531 120	Multimeter LD analog 20	1	1
460 34	Auxiliary bench with swivel joint	1	
460 32	Precision optical bench, standardized cross section, 1 m		1
460 373	Optics rider, $H = 60$ mm/ $W = 50$ mm	1	1
460 374	Optics rider, $H = 90$ mm/ $W = 50$ mm	1	1
460 375	Optics rider, $H = 120$ mm/ $W = 50$ mm	3	3
460 380	Cantilever arm	1	1
590 011	Clamping plug	2	2
501 10	Straight BNC	1	1
501 09	BNC adapter for 4 mm socket, 1-pole	1	1
340 89	Coupling plug	1	1
500 440	Connection lead, yellow-green, 100 cm	2	2
501 45	Pair of cables, 50 cm, red and blue	1	1
502 04	Distribution box	1	1

In determining Planck's constant using the photoelectric effect, it must be ensured that only the light of a single spectral line of the high-pressure mercury vapor lamp falls on the cathode of the photocell at any one time. As an alternative to a prism, it is also possible to use narrow-band interference filters to select the wavelength. This simplifies the subsequent optical arrangement, and it is no longer necessary to darken the experiment room. Also, the intensity of the light incident on the cathode can be easily varied using an iris diaphragm.

In this experiment, the capacitor method described previously (see P 6.1.4.1) is used to generate the opposing voltage U between the cathode and the anode of the photocell. The voltage at the capacitor is measured without current using the electrometer amplifier.

Note: The opposing voltage U can alternatively be tapped from a DC voltage source. The I-measuring amplifier D is recommended for sensitive measurements of the anode current (see P 6.1.4.2).

P 6.1.5**Dualism of wave and particle**

- P 6.1.5.1 Diffraction of electrons in a polycrystalline lattice (Debye-Scherrer diffraction)
- P 6.1.5.2 Optical analogy to diffraction of electrons in a polycrystalline lattice



Diffraction of electrons in a polycrystalline lattice (Debye-Scherrer diffraction) (P 6.1.5.1)

In 1924, *L. de Broglie* first hypothesized that particles could have wave properties in addition to their familiar particle properties, and that their wavelength depends on the linear momentum p

$$\lambda = \frac{h}{p} \quad h: \text{Planck's constant}$$

His conjecture was confirmed in 1927 by the experiments of *C. Davisson* and *L. Germer* on the diffraction of electrons at crystalline structures.

The first experiment demonstrates diffraction of electrons at polycrystalline graphite. As in the Debye-Scherrer method with x-rays, we observe diffraction rings in the direction of radiation which surround a central spot on a screen. These are caused by the diffraction of electrons at the lattice planes of microcrystals which fulfill the Bragg condition

$$2 \cdot d \cdot \sin \vartheta = n \cdot \lambda$$

ϑ : angular aperture of diffraction ring

d : spacing of lattice planes

As the graphite structure contains two lattice-plane spacings, two diffraction rings in the first order are observed. The electron wavelength

$$\lambda = \frac{h}{\sqrt{2 \cdot m_e \cdot e \cdot U}}$$

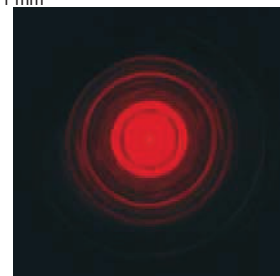
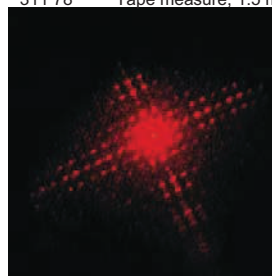
m_e : mass of electron, e : elementary charge

is determined by the acceleration voltage U , so that for the angular aperture of the diffraction rings we can say

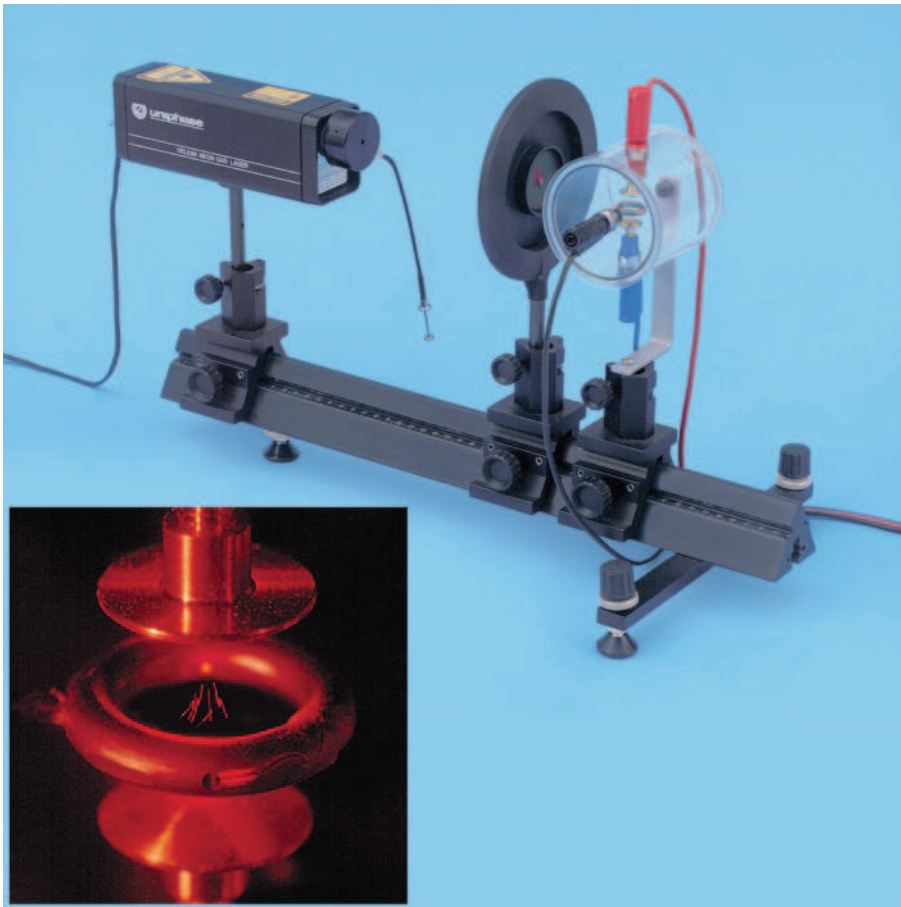
$$\sin \vartheta \propto \frac{1}{\sqrt{U}}$$

The second experiment illustrates the Debye-Scherrer method used in the electron diffraction tube by means of visible light. Here, parallel, monochromatic light passes through a rotating cross grating. The diffraction pattern of the cross grating at rest, consisting of spots of light arranged around the central beam in a network-like pattern, is deformed by rotation into rings arranged concentrically around the central spot.

Cat. No.	Description	P 6.1.5.1	P 6.1.5.2
555 626	Electron diffraction tube	1	
555 600	Stand rod for electron tubes	1	
521 70	High voltage power supply 10 kV	1	
311 54	Precision vernier callipers	1	
555 629	Cross grating, rotatable		1
450 63	Halogen lamp, 12 V/100 W		1
450 64	Halogen lamp housing, 12 V, 50/100 W		1
450 66	Picture slider for halogen lamp housing		1
521 25	Transformer 2 ... 12 V		1
460 22	Holder with spring clips		1
460 03	Lens $f = +100$ mm		1
441 53	Translucent screen		1
460 43	Small optical bench		1
301 01	Leybold multiclamp		5
300 01	Stand base, V-shape, 28 cm		1
501 46	Pair of cables, 1 m, red and blue		1
500 611	Safety connection lead, 25 cm, red	1	
500 621	Safety connection lead, 50 cm, red	1	
500 641	Safety connection lead, 100 cm, red	1	
500 642	Safety connection lead, 100 cm, blue	1	
500 644	Safety connection lead, 100 cm, black	2	
311 78	Tape measure, 1.5 m/1 mm		1



Optical analogon of Debye-Scherrer diffraction (P 6.1.5.2)

**P 6.1.6****Paul trap**

P 6.1.6.1 Observing individual lycopod spores in a Paul trap

Observing individual lycopod spores in a Paul trap (P 6.1.6.1)

Cat. No.	Description	P 6.1.6.1 (a)	P 6.1.6.1 (b)
558 80	Paul trap	1	1
471 830	He-Ne laser, linearly polarized	1	1
460 01	Lens $f = + 5 \text{ mm}$	1	1
460 34	Auxiliary bench w. swivel joint, 0.5 m	1	
460 32	Precision optical bench, standardized cross section, 1 m		1
460 373	Optics rider, $H = 60 \text{ mm}/W = 50 \text{ mm}$	3	3
522 27	Power supply 450 V DC	1	1
521 35	Variable extra low voltage transformer S	1	1
562 11	U-core with yoke	1	1
562 12	Clamping device	1	1
562 18	Extra-low voltage coil, 50 turns	1	1
562 16	Coil with 10,000 turns	1	1
531 120	Multimeter LDanalog 20	1	1
536 211	Measuring resistor 10 M Ω , 1 W	1	1
500 644	Safety connection lead, 100 cm, black	1	1
500 624	Safety connection lead, 50 cm, black	2	2
500 641	Safety connection lead, 100 cm, red	1	1
500 642	Safety connection lead, 100 cm, blue	1	1
500 98	Set of 6 safety adapter sockets, black	1	1
501 45	Pair of cables, 50 cm, red and blue	2	2
500 440	Connection lead, 100 cm, yellow/green	1	1
502 04	Distribution box	1	1

Spectroscopic measurements of atomic energy levels are normally impaired by the motion of the atoms under study with respect to the radiation source. This motion shifts and broadens the spectral lines due to the Doppler effect, which becomes strongly apparent in high-resolution spectroscopy. The influence of the Doppler effect is reduced when individual atoms are enclosed in a small volume for spectroscopic measurements. For charged particles (ions), this can be achieved using the ion trap developed by W. Paul in the 1950's. This consists of two rotationally symmetrical cover electrodes and one ring electrode. The application of an AC voltage generates a time-dependent, parabolic potential with the form

$$U(r, z, t) = U_0 \cdot \cos \omega t \cdot \frac{r^2 - 2z^2}{2 \cdot r_0^2}$$

z : coordinate on the axis of symmetry,
 r : coordinate perpendicular to axis of symmetry,
 r_0 : inside radius of ring electrode

An ion with the charge q and the mass m remains trapped in this potential when the conditions

$$0.4 \cdot \alpha < \frac{q}{m} < 1.2 \cdot \alpha \text{ where } \alpha = \frac{r_0^2 \cdot \omega^2}{U_0}$$

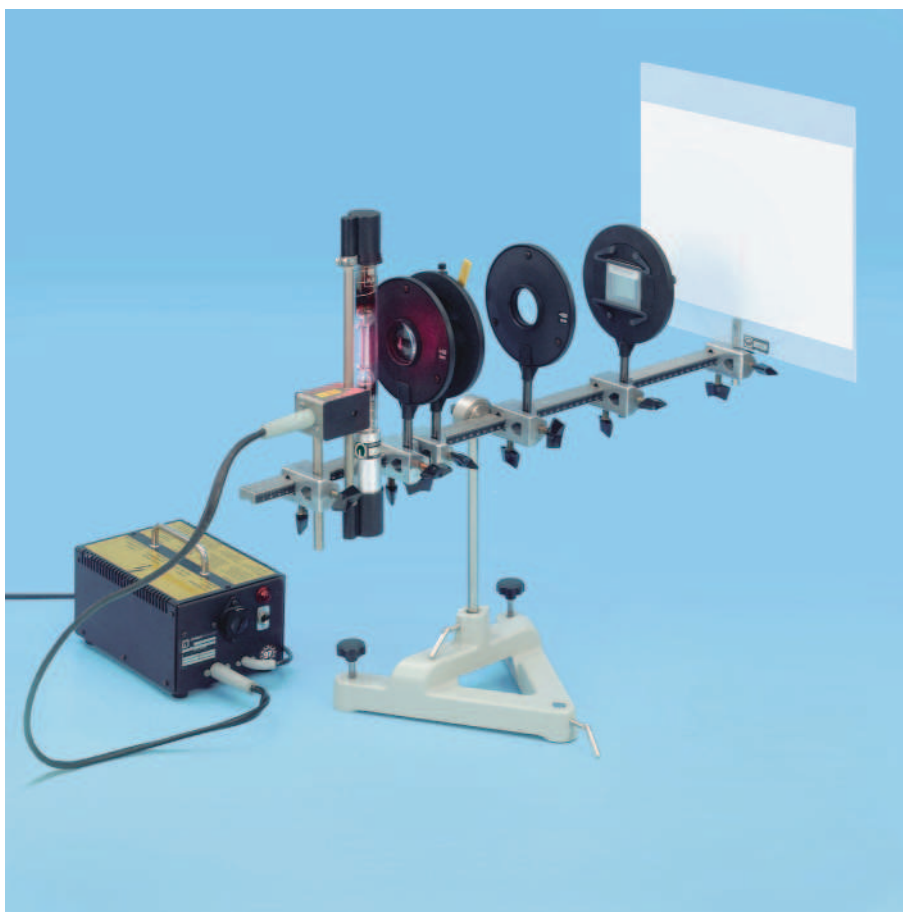
are fulfilled.

This experiment demonstrates how a Paul trap works using a model which can be operated with no special requirements at standard air pressure and with 50 Hz AC. When a suitable voltage amplitude U_0 is set, it is possible to trap lycopod spores for several hours and observe them under laser light. Tilting of the entire ion trap causes the trapped particles to move radially within the ring electrode. When a voltage is applied between the cover electrodes, it is possible to shift the potential along the z -axis.

P 6.2.1

The Balmer series of hydrogen

- P 6.2.1.1 Determining the wavelengths H_{α} , H_{β} and H_{γ} from the Balmer series of hydrogen
- P 6.2.1.2 Observing the Balmer series of hydrogen using a prism spectrometer

Determining the wavelengths H_{α} , H_{β} and H_{γ} from the Balmer series of hydrogen (P 6.2.1.1)

In the visible range, the emission spectrum of atomic hydrogen has four lines, H_{α} , H_{β} , H_{γ} and H_{δ} ; this sequence continues into the ultraviolet range to form a complete series. In 1885, *Balmer* empirically worked out a formula for the frequencies of this series

$$\nu = R_{\infty} \cdot \left(\frac{1}{2^2} - \frac{1}{m^2} \right), \quad m: 3, 4, 5, \dots$$

$$R_{\infty} = 3.2899 \cdot 10^{15} \text{ s}^{-1}: \text{Rydberg constant}$$

which could later be explained using Bohr's model of the atom.

In this experiment, the emission spectrum is excited using a Balmer lamp filled with water vapor, in which an electric discharge splits the water molecules into an excited hydrogen atom and a hydroxyl group. The wavelengths of the lines H_{α} , H_{β} and H_{γ} are determined using a high-resolution grating. In the first diffraction order of the grating, we can find the following relationship between the wavelength λ and the angle of observation ϑ :

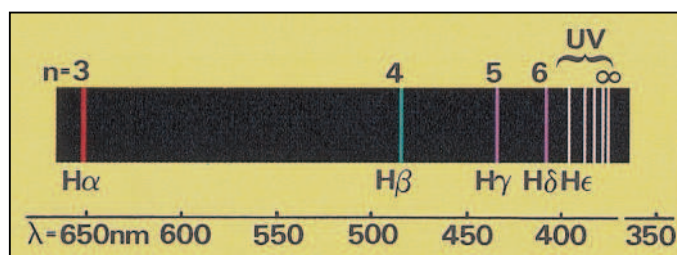
$$\lambda = d \cdot \sin \vartheta$$

d : grating constant

The measured values are compared with the values calculated according to the Balmer formula.

In the second experiment the Balmer series are studied by means of a prism spectroscope (complete device).

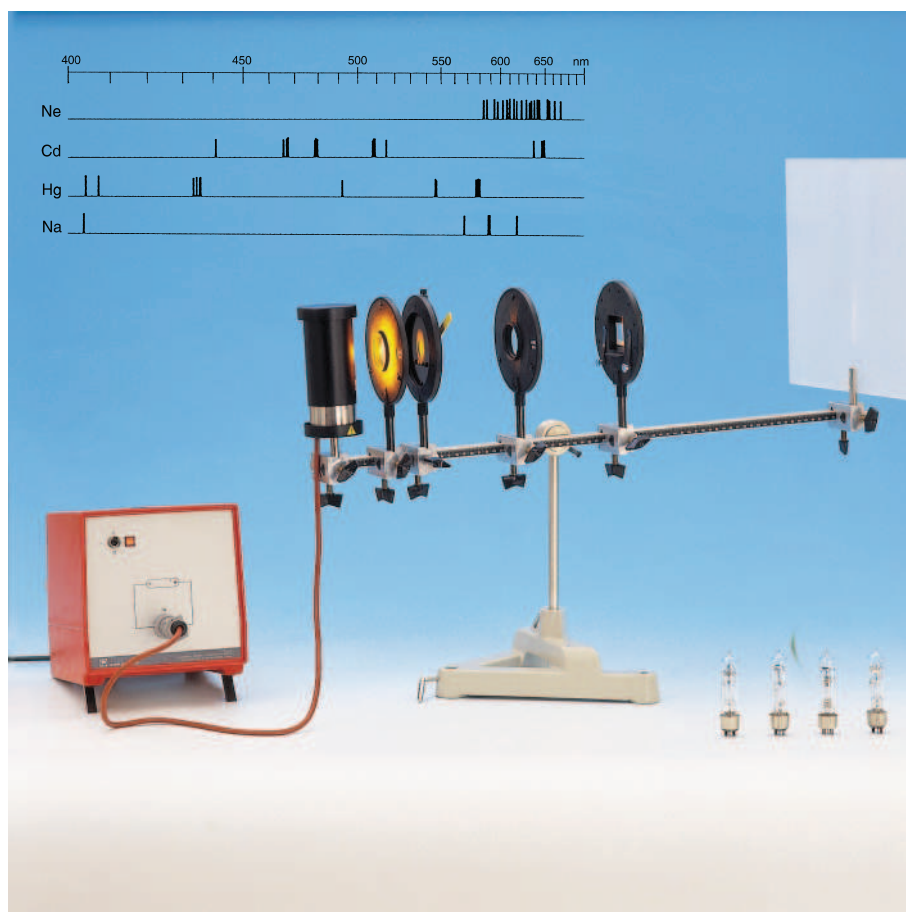
Cat. No.	Description	P 6.2.1.1	P 6.2.1.2
451 13	Balmer lamp	1	1
451 14	Power supply unit for Balmer lamps	1	1
471 23	Copy of a Rowland grating, approx. 5700 lines/cm	1	
311 77	Steel tape measure, 2 m	1	
460 02	Lens $f = + 50 \text{ mm}$	1	
460 03	Lens $f = + 100 \text{ mm}$	1	
460 14	Adjustable slit	1	
460 22	Holder with spring clips	1	
441 53	Translucent screen	1	
460 43	Small optical bench	1	
300 01	Stand base, V-shape, 28 cm	1	
301 01	Leybold multiclamp	6	
467 112	School spectroscope		1



Emission spectrum of atomic hydrogen



Observing the Balmer series of hydrogen using a prism spectrometer (P 6.2.1.2)



Displaying the line spectra of inert gases and metal vapors (P 6.2.2.1)

P 6.2.2**Emission and absorption spectra**

P 6.2.2.1 Displaying the line spectra of inert gases and metal vapors

P 6.2.2.2 Qualitative investigation of the absorption spectrum of sodium

Cat. No.	Description	P 6.2.2.1	P 6.2.2.2
451 011	Spectral lamp Ne	1	
451 041	Spectral lamp Cd	1	
451 062	Spectral lamp Hg 100	1	
451 111	Spectral lamp Na	1	1
451 16	Housing for spectral lamps with pin contact	1	1
451 30	Universal choke 230 V, 50 Hz	1	1
460 02	Lens $f = + 50$ mm	1	
460 03	Lens $f = + 100$ mm	1	
471 23	Copy of a Rowland grating, approx. 5700 lines/cm	1	
460 14	Adjustable slit	1	
460 22	Holder with spring clips	1	
441 53	Translucent screen	1	1
311 77	Steel tape measure, 2 m	1	
460 43	Small optical bench	1	
300 01	Stand base, V-shape, 28 cm	1	
301 01	Leybold multiclamp	6	2
673 5700	Sodium chloride, 250 g		1
666 962	Spatula, double-ended, 150 mm, 9 mm wide, stainless steel		1
666 711	Butane gas burner, gas and air regulation valve		1
666 712	Butane gas cartridges, 200 g, set of 3, for 666 711/713		1
450 60	Lamp housing		1
450 51	Lamp, 6 V/30 W		1
521 210	Transformer, 6 V AC, 12 V AC/30 VA		1
300 02	Stand base, V-shape, 20 cm		2
300 11	Saddle base		1
300 42	Stand rod, 47 cm		2
673 0840	Magnesia rods, set of 25		1

When an electron in the shell of an atom or atomic ion drops from an excited state with the energy E_2 to a state of lower energy E_1 , it can emit a photon with the frequency

$$\nu = \frac{E_2 - E_1}{h}$$

h : Planck's constant

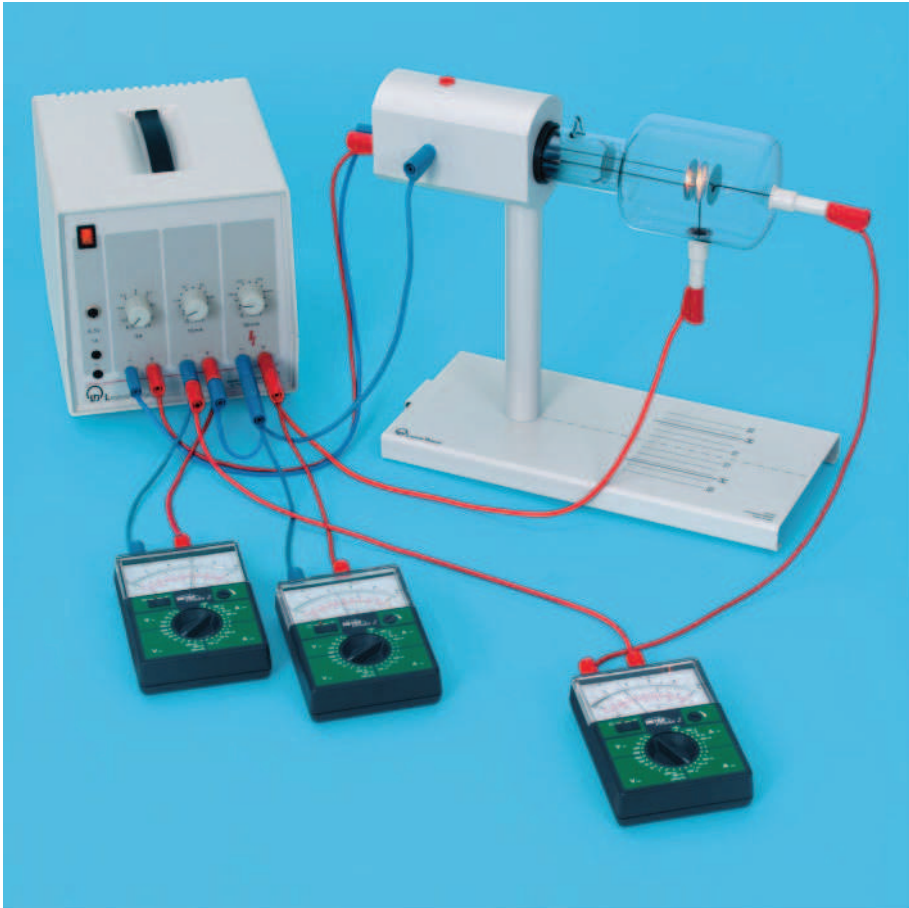
In the opposite case, a photon with the same frequency is absorbed. As the energies E_1 and E_2 can only assume discrete values, the photons are only emitted and absorbed at discrete frequencies. The totality of the frequencies which occur is referred to as the spectrum of the atom. The positions of the spectral lines are characteristic of the corresponding element.

The first experiment disperses the emission spectra of metal vapors and inert gases (mercury, sodium, cadmium and neon) using a high-resolution grating and projects these on the screen for comparison purposes.

In the second experiment, the flame of a Bunsen burner is alternately illuminated with white light and sodium light and observed on a screen. When sodium is burned in the flame, a dark shadow appears on the screen when illuminating with sodium light. From this it is possible to conclude that the light emitted by a sodium lamp is absorbed by the sodium vapor, and that the same atomic components are involved in both absorption and emission.

P 6.2.3
Inelastic electron collisions

P 6.2.3.1 Discontinuous energy emission
of electrons in a gas-filled triode

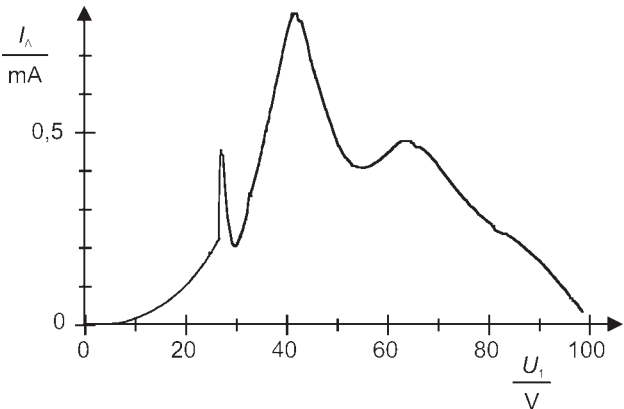


Discontinuous energy emission of electrons in a gas-filled triode (P 6.2.3.1)

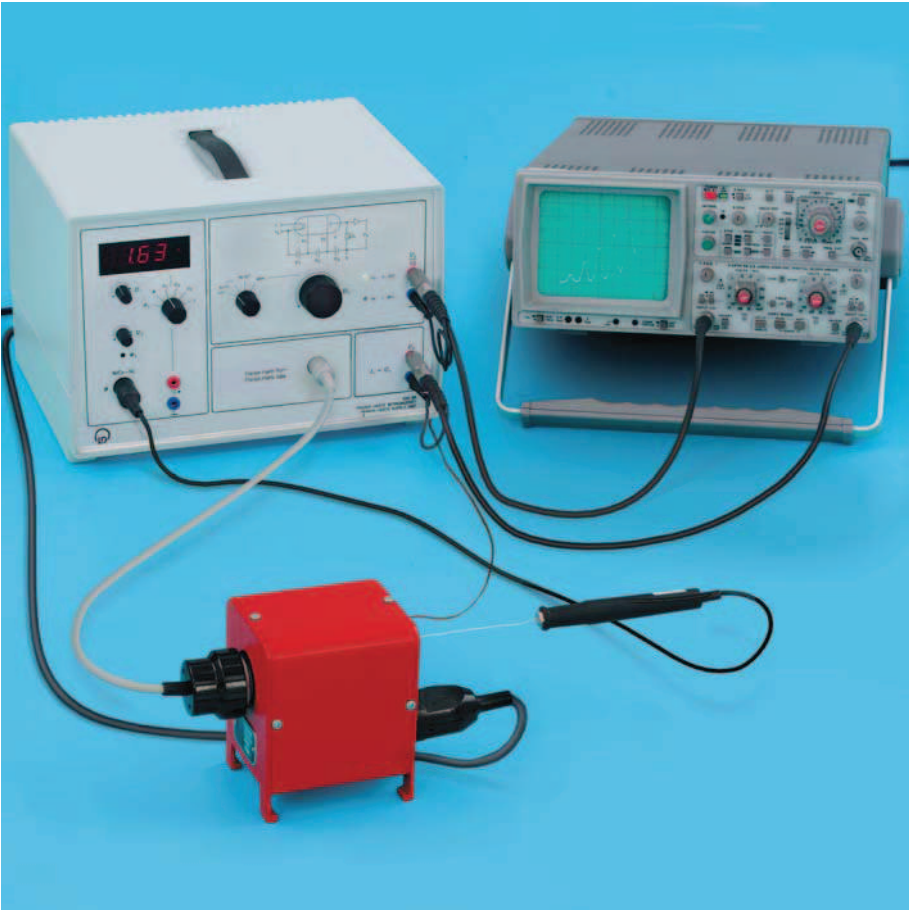
In inelastic collision of an electron with an atom, the kinetic energy of the electron is transformed into excitation or ionization energy of the atom. Such collisions are most probable when the kinetic energy is exactly equivalent to the excitation or ionization energy. As the excitation levels of the atoms can only assume discrete values, the energy emission in the event of inelastic electron collision is discontinuous.

This experiment uses a tube triode filled with helium to demonstrate this discontinuous emission of energy. After acceleration in the electric field between the cathode and the grid, the electrons enter an opposing field which exists between the grid and the anode. Only those electrons with sufficient kinetic energy reach the anode and contribute to the current I flowing between the anode and ground. Once the electrons in front of the grid have reached a certain minimum energy (which depends on the gas), they can excite the gas atoms through inelastic collision. When the acceleration voltage U is continuously increased, the inelastic collisions initially occur directly in front of the grid, as the kinetic energy of the electrons reaches its maximum value here. After collision, the electrons can no longer travel against the opposing field. The anode current I is thus greatly decreased. When the acceleration voltage U is increased further, the excitation zone moves toward the cathode, the electrons can again accumulate energy on their way to the grid and the current I again increases. Finally, the electrons can excite gas atoms a second time, and the anode current drops once more.

Cat. No.	Description	P 6.2.3.1
555 614	Gas filled triode	1
555 600	Stand for electron tubes	1
521 65	DC power supply 0 ... 500 V	1
531 120	Voltmeter, DC, $U < 100$ V, e.g. Multimeter LDanalog 20	2
531 120	Amperemeter, DC, $I < 100$ μ A, e.g. Multimeter LDanalog 20	1
500 621	Safety connection lead, 50 cm, red	1
500 641	Safety connection lead, 100 cm, red	4
500 642	Safety connection lead, 100 cm, blue	6



Anode current I as a function of the acceleration voltage U for He



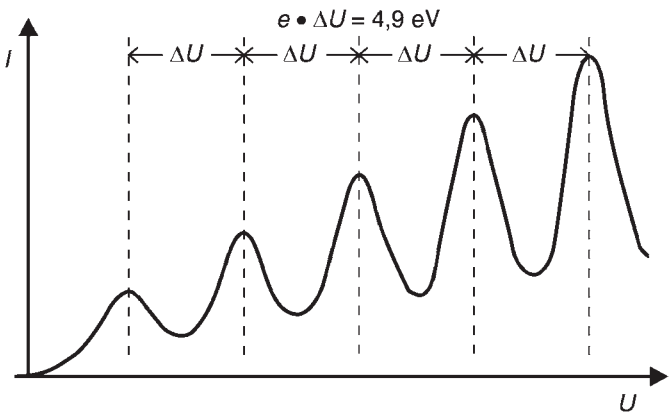
P 6.2.4

Franck-Hertz experiment

- P 6.2.4.1 Franck-Hertz experiment with mercury – recording with the oscilloscope, the XY recorder or point by point
- P 6.2.4.2 Franck-Hertz experiment with mercury – measuring and evaluating with CASSY

Franck-Hertz experiment with mercury – recording with the oscilloscope (P 6.2.4.1 b)

Cat. No.	Description	P 6.2.4.1(a)	P 6.2.4.1(b)	P 6.2.4.1(c)	P 6.2.4.2
555 854	Mercury Franck-Hertz tube	1	1	1	1
555 864	Socket for Franck-Hertz-tube with multi-pin plug	1	1	1	1
555 81	Electric oven, 230 V	1	1	1	1
555 880	Franck-Hertz supply unit	1	1	1	1
666 193	Temperature sensor NiCr-Ni	1	1	1	1
575 211	Two-channel oscilloscope 303		1		
575 24	Screened cable BNC/4 mm		2		
575 664	XY-Yt recorder			1	
501 46	Pair of cables, 1 m, red and blue			2	2
524 010USB	Sensor CASSY				1
524 200	CASSY Lab				1
	additionally required: PC with Windows 95/98/NT or higher				1



Franck-Hertz curve

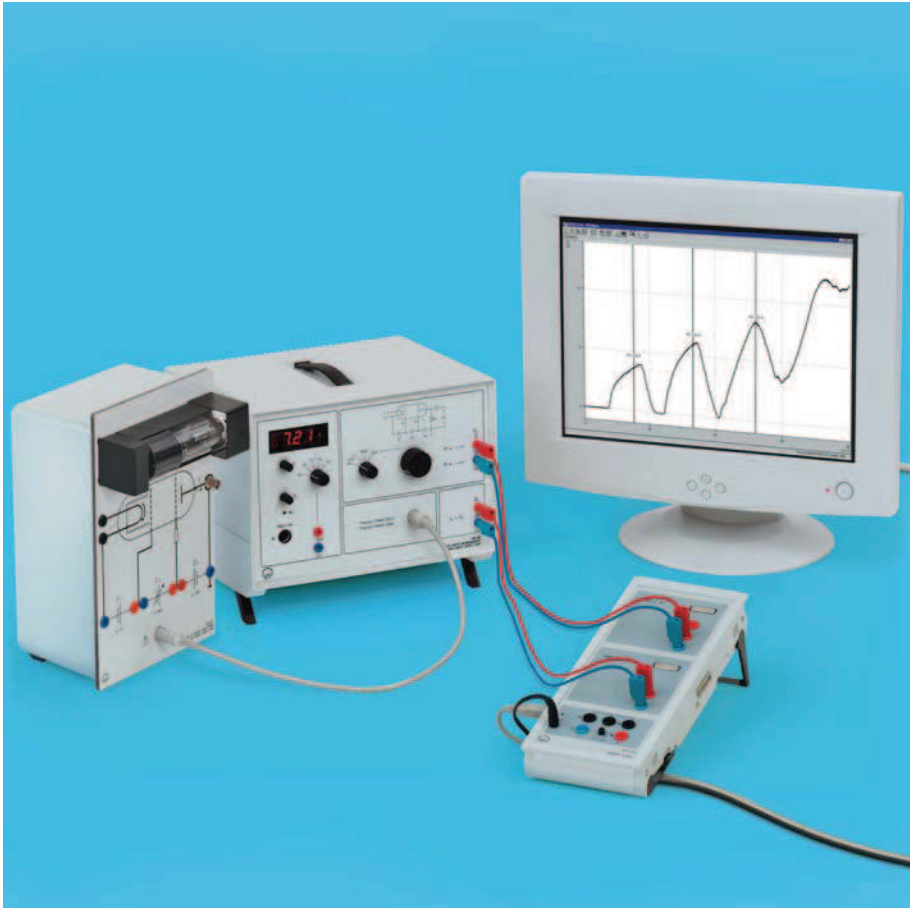
In 1914, *J. Franck* and *G. Hertz* reported observing discontinuous energy emission when electrons passed through mercury vapor, and the resulting emission of the ultraviolet spectral line ($\lambda = 254 \text{ nm}$) of mercury. A few months later, *Niels Bohr* recognized that their experiment supported his model of the atom.

This experiment is offered in two variations, which differ only in the means of recording and evaluating the measurement data. The mercury atoms are enclosed in a tetrode with cathode, grid-type control electrode, acceleration grid and target electrode. The control grid ensures a virtually constant emission current of the cathode. An opposing voltage is applied between the acceleration grid and the target electrode. When the acceleration voltage U between the cathode and the acceleration grid is increased, the target current I corresponds closely to the tube characteristic once it rises above the opposing voltage. As soon as the electrons acquire sufficient kinetic energy to excite the mercury atoms through inelastic collisions, the electrons can no longer reach the target, and the target current drops. At this acceleration voltage, the excitation zone is directly in front of the excitation grid. When the acceleration voltage is increased further, the excitation zone moves toward the cathode, the electrons can again accumulate energy on their way to the grid and the target current again increases. Finally, the electrons can excite the mercury atoms once more, the target current drops again, and so forth. The $I(U)$ characteristic thus demonstrates periodic variations, whereby the distance between the minima $\Delta U = 4.9 \text{ V}$ corresponds to the excitation energy of the mercury atoms from the ground state 1S_0 to the first 3P_1 state.

P 6.2.4

Franck-Hertz experiment

- P 6.2.4.3 Franck-Hertz experiment with neon – recording with the oscilloscope, the XY recorder or point by point
- P 6.2.4.4 Franck-Hertz experiment with neon – measuring and evaluating with CASSY

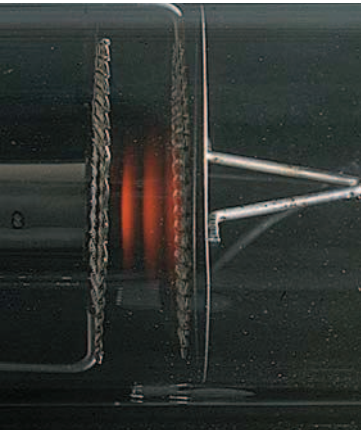


Franck-Hertz experiment with neon (P 6.2.4.4)

When neon atoms are excited by means of inelastic electron collision at a gas pressure of approx. 10 hPa, excitation is most likely to occur to states which are 18.7 eV above the ground state. The de-excitation of these states can occur indirectly via intermediate states, with the emission of photons. In this process, the photons have a wavelength in the visible range between red and green. The emitted light can thus be observed with the naked eye and e.g. measured using the school spectroscope Kirchhoff/Bunsen (467 112).

The Franck-Hertz experiment with neon is offered in two variations, which differ only in the means of recording and evaluating the measurement data. In both variations, the neon atoms are enclosed in a glass tube with four electrodes: the cathode K, the grid-type control electrode G_1 , the acceleration grid G_2 and the target electrode A. Like the Franck-Hertz experiment with mercury, the acceleration voltage U is continuously increased and the current I of the electrons which are able to overcome the opposing voltage between G_2 and A and reach the target is measured. The target current is always lowest when the kinetic energy directly in front of grid G_2 is just sufficient for collision excitation of the neon atoms, and increases again with the acceleration voltage. We can observe clearly separated luminous red layers between grids G_1 and G_2 ; their number increases with the voltage. These are zones of high excitation density, in which the excited atoms emit light in the visible spectrum.

Cat. No.	Description	P 6.2.4.3(a)	P 6.2.4.3(b)	P 6.2.4.3(c)	P 6.2.4.4
555 870	Neon Franck-Hertz tube	1	1	1	1
555 871	Holder with socket and screen for neon FH tube	1	1	1	1
555 872	Connecting cable for Ne-FH	1	1	1	1
555 880	Franck-Hertz supply unit	1	1	1	1
575 211	Two-channel oscilloscope 303		1		
575 24	Screened cable BNC/4 mm		2		
575 664	XY-Yt recorder			1	
524 010USB	Sensor CASSY				1
524 200	CASSY Lab				1
501 46	Pair of cables, 1 m, red and blue			2	2
	additionally required: PC with Windows 95/98/NT or higher				1



Luminous layers between control electrode and acceleration grid



P 6.2.6**Electron spin resonance (ESR)**

- P 6.2.6.2 Electron spin resonance in DPPH – determining the magnetic field as a function of the resonance frequency
- P 6.2.6.3 Resonance absorption of a passive RF oscillator circuit



Electron spin resonance in DPPH – determining the magnetic field as a function of the resonance frequency (P 6.2.6.2)

The magnetic moment of the unpaired electron with the total angular momentum j in a magnetic field assumes the discrete energy states

$$E_m = -g_j \cdot \mu_B \cdot m \cdot B \text{ where } m = -j, -j+1, \dots, j$$

$$\mu_B = 9,274 \cdot 10^{-24} \frac{\text{J}}{\text{T}}: \text{Bohr's magneton}$$

g_j : g factor

When a high-frequency magnetic field with the frequency ν is applied perpendicularly to the first magnetic field, it excites transitions between the adjacent energy states when these fulfill the resonance condition

$$h \cdot \nu = E_{m+1} - E_m$$

h : Planck's constant.

This fact is the basis for electron spin resonance, in which the resonance signal is detected using radio-frequency technology. The electrons can often be regarded as free electrons. The g -factor then deviates only slightly from that of the free electron ($g = 2.0023$), and the resonance frequency ν in a magnetic field of 1 mT is about 27.8 MHz. The actual aim of electron spin resonance is to investigate the internal magnetic fields of the sample substance, which are generated by the magnetic moments of the adjacent electrons and nuclei.

The first experiment verifies electron spin resonance in diphenylpicryl-hydrazyl (DPPH). DPPH is a radical, in which a free electron is present in a nitrogen atom. In the experiment, the magnetic field B which fulfills the resonance condition the resonance frequencies ν can be set in a continuous range from 13 to 130 MHz. The aim of the evaluation is to determine the g factor.

The object of the final experiment is to verify resonance absorption using a passive oscillator circuit.

Cat. No.	Description	P 6.2.6.2	P 6.2.6.3
514 55	ESR basic unit	1	1
514 571	ESR control unit	1	1
555 604	Pair of Helmholtz coils	1	
575 211	Two-channel oscilloscope 303	1	1
501 02	BNC cable, 1 m	2	
575 24	Screened cable BNC/4 mm		1
501 644	Set 6 two-way adapters, black		1
	Ammeter, DC, $I \leq 1$ mA, e.g.		
531 120	Multimeter LD analog 20		1
300 11	Stand base	3	2
590 13	Insulated stand rod, 25 cm		1
501 23	Connecting lead, \varnothing 2.5 mm2, 25 cm, black	1	
501 25	Connecting lead, \varnothing 2.5 mm2, 50 cm, red	1	
501 26	Connecting lead, \varnothing 2.5 mm2, 50 cm, blue	1	

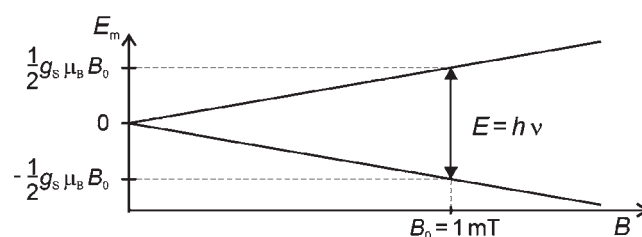
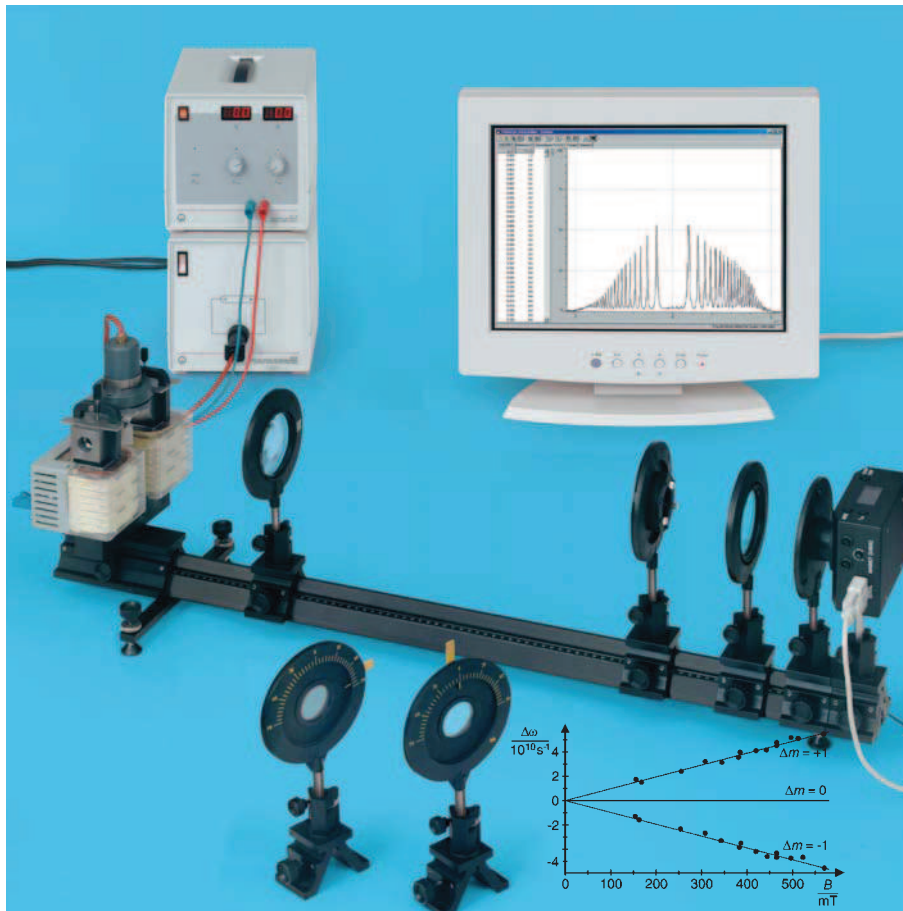


Diagram of resonance condition of free electrons



Measuring the Zeeman split of the red cadmium line as a function of the magnetic field (P 6.2.7.4)

P 6.2.7**Normal Zeeman effect**

- P 6.2.7.1 Observing the normal Zeeman effect in transverse and longitudinal configuration – spectroscopy using a Lummer-Gehrcke plate
- P 6.2.7.2 Measuring the Zeeman split of the red cadmium line as a function of the magnetic field – spectroscopy using a Lummer-Gehrcke plate
- P 6.2.7.3 Observing the normal Zeeman effect in transverse and longitudinal configuration – spectroscopy using a Fabry-Perot etalon
- P 6.2.7.4 Measuring the Zeeman split of the red cadmium line as a function of the magnetic field – spectroscopy using a Fabry-Perot etalon

Cat. No.	Description	P 6.2.7.1	P 6.2.7.2(a)	P 6.2.7.2(b)	P 6.2.7.3(a)	P 6.2.7.3(b)	P 6.2.7.4(a)	P 6.2.7.4(b)
451 12	Cadmium lamp for Zeeman-Effekt	1	1	1	1	1	1	1
451 30	Universal choke, in housing, 230 V, 50 Hz	1	1	1	1	1	1	1
521 55	High current power supply	1	1	1	1	1	1	1
514 50	Electromagnet for Zeeman-Effekt	1	1	1				
471 20	Optical system for observing the Zeeman-Effekt	1	1	1				
471 21	Lummer-Gehrcke plate	1	1	1				
562 11	U-core with yoke				1	1	1	1
562 131	Coil, 10 A, 480 turns				2	2	2	2
560 315	Pair of pole pieces with great bore				1	1	1	1
471 221	Fabry-Perot etalon				1	1	1	1
460 32	Precision optical bench, stand. cross section, 1 m				1	1	1	1
460 381	Rider base, Width: 148 mm				1	1	1	1
460 373	Optics rider, H = 60 mm/W = 50 mm				7	7	5	5
460 08	Lens, f = + 150 mm				2	2	2	2
472 601	Quarter-wavelength plate				1	1		
472 401	Polarization filter				1	1		
460 22	Holder with spring clips				1			
467 95	Filter set red, green, blue				1			
468 41	Holder for interference filters					1	1	1
468 400	Interference filter, 644 nm					1	1	1
460 135	Ocular with scale				1	1		
337 47USB	VideoCom USB						1	1
531 835	Universal Measuring Instrument Physics	1					1	
524 0381	Combi B-Sensor S	1	1				1	1
501 11	Extension cable, 15-pole	1	1				1	1
300 02	Stand base, V-shape, 20 cm	1	1				1	1
300 42	Stand rod, 47 cm	1	1				1	1
301 01	Leybold multiclamp	1	1				1	1
501 33	Connecting lead, Ø 2.5 mm ² , 100 cm, black				3	3	3	3
501 20	Connecting lead, Ø 2.5 mm ² , 25 cm, red	1	1	1				
501 21	Connecting lead, Ø 2.5 mm ² , 25 cm, blue	1	1	1				
501 30	Connecting lead, Ø 2.5 mm ² , 100 cm, red	1	1	1				
501 31	Connecting lead, Ø 2.5 mm ² , 100 cm, blue	1	1	1				
required: PC with Windows 95/98/NT or higher							1	1

The Zeeman effect is the name for the splitting of atomic energy levels in an external magnetic field and, as a consequence, the splitting of the transitions between the levels. The effect was predicted by *H. A. Lorentz* in 1895 and experimentally confirmed by *P. Zeeman* one year later. In the red spectral line of cadmium ($\lambda = 643.8$ nm), Zeeman observed a line triplet perpendicular to the magnetic field and a line doublet parallel to the magnetic field, instead of just a single line. Later, even more complicated splits were discovered for other elements, and were collectively designated the anomalous Zeeman effect. It eventually became apparent that the normal Zeeman effect is the exception, as it only occurs at transitions between atomic levels with the total spin $S = 0$.

In the first and third experiment, the Zeeman effect is observed at the red cadmium line perpendicular and parallel to the magnetic field, and the polarization state of the individual Zeeman components is determined. The observations are explained on the basis of the radiating characteristic of dipole radiation. The so-called π component corresponds to a Hertzian dipole oscillating parallel to the magnetic field, i. e. it cannot be observed parallel to the magnetic field and radiates linearly polarized light perpendicular to the magnetic field. Each of the two σ components corresponds to two dipoles oscillating perpendicular to each other with a phase differential of 90° . They radiate circularly polarized light in the direction of the magnetic field and linearly polarized light parallel to it.

In the second and fourth experiment, the Zeeman splitting of the red cadmium line is measured as a function of the magnetic field B . The energy interval of the triplet components

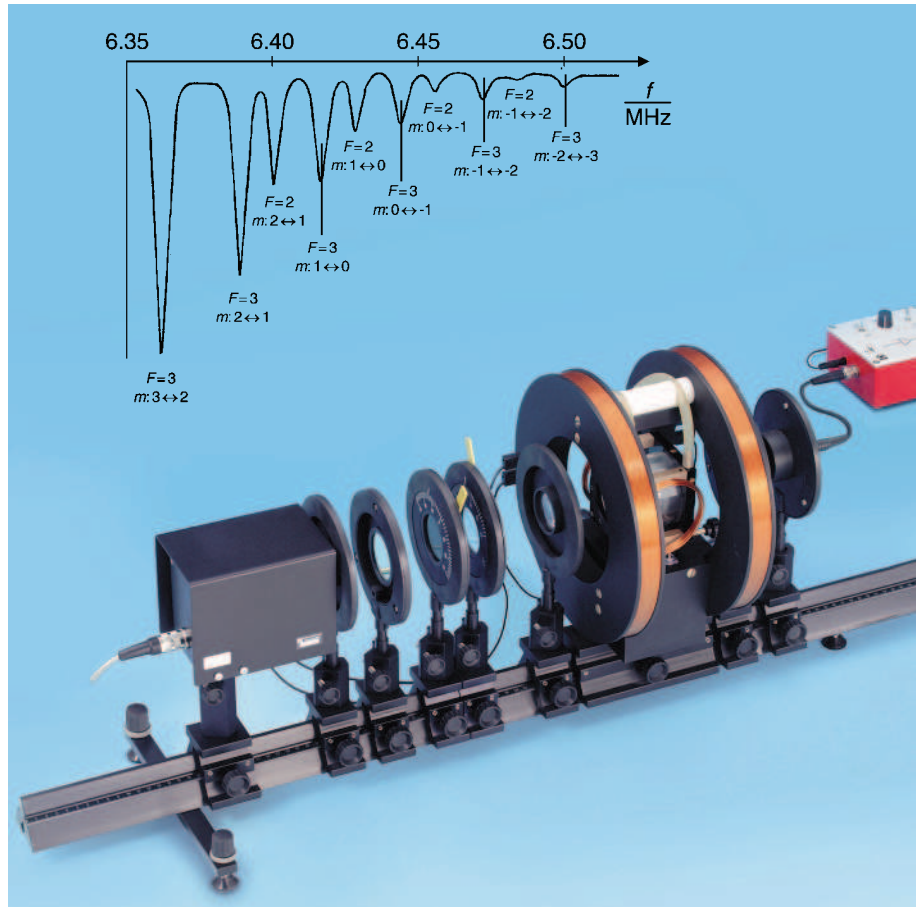
$$\Delta E = \frac{h}{4\pi} \cdot \frac{e}{m_e} \cdot B$$

m_e : mass of electron, e : electron charge,
 h : Planck's constant
 B : magnetic induction

is used to calculate the specific electron charge.

P 6.2.8**Optical pumping
(anomalous Zeeman effect)**

- P 6.2.8.1 Optical pumping:
observing the pumping signal
- P 6.2.8.2 Optical pumping:
measuring and observing the
Zeeman transitions in the
ground state of Rb-87 with σ^+
and σ^- pumped light
- P 6.2.8.3 Optical pumping:
measuring and observing the
Zeeman transitions in the
ground state of Rb-85 with σ^+
and σ^- pumped light
- P 6.2.8.4 Optical pumping:
measuring and observing the
Zeeman transitions in the
ground state of Rb-87 as a
function of the magnetic flux
density B
- P 6.2.8.5 Optical pumping:
measuring and observing the
Zeeman transitions in the
ground state of Rb-85 as a
function of the magnetic flux
density B
- P 6.2.8.6 Optical pumping:
measuring and observing two-
quantum transitions

Measuring and observing the Zeeman transitions in the ground state of Rb-87 with σ^+ pumped light (P 6.2.8.2)

The two hyperfine structures of the ground state of an alkali atom with the total angular momentums

$$F_+ = I + \frac{1}{2}, F_- = I - \frac{1}{2}$$

split in a magnetic field B into $2F_{\pm} + 1$ Zeeman levels having an energy which can be described using the *Breit-Rabi* formula

$$E = \frac{-\Delta E}{2(2I + 1)} + \mu_K g_I m_F \pm \frac{\Delta E}{2} \sqrt{1 + \frac{4m_F}{2I + 1} \xi + \xi^2}$$

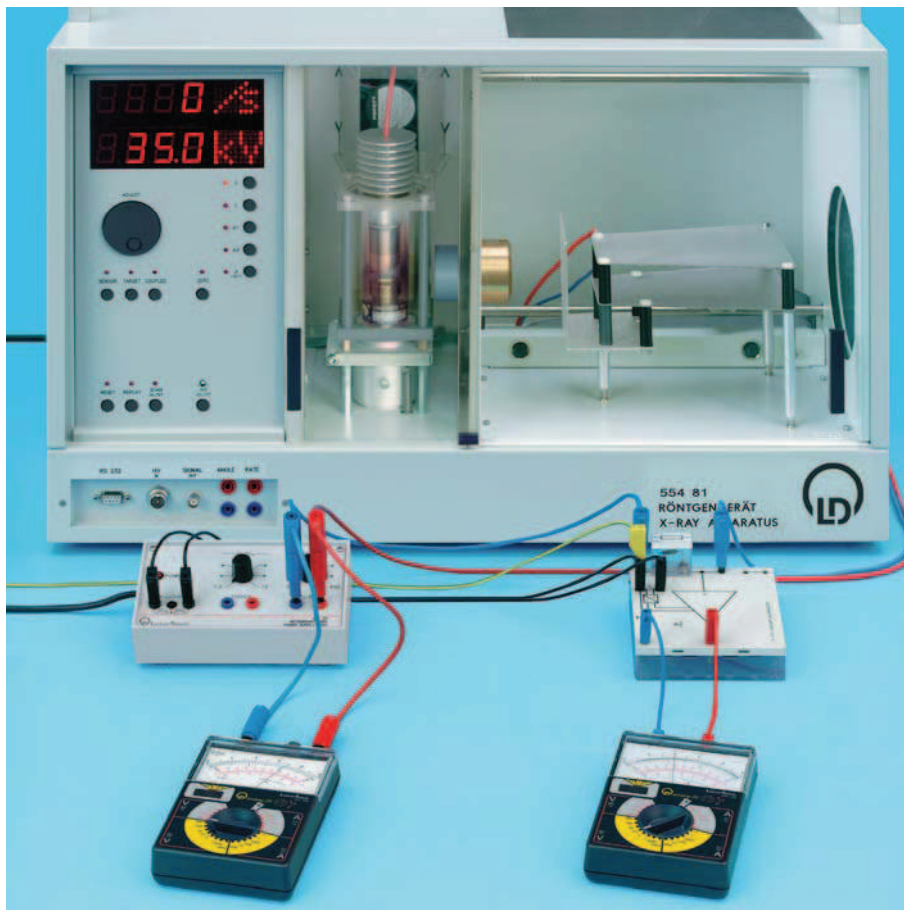
$$\text{where } \xi = \frac{g_J \mu_B - g_I \mu_K}{\Delta E} \cdot B$$

ΔE : hyperfine structure interval,
 I : nuclear spin, m_F : magnetic quantum number,
 μ_B : Bohr's magneton, μ_K : nuclear magneton,
 g_J : shell g factor, g_I : nuclear g factor

Transitions between the Zeeman levels can be observed using a method developed by A. Kastler. When right-handed or left-handed circularly polarized light is directed parallel to the magnetic field, the population of the Zeeman level differs from the thermal equilibrium population, i.e. optical pumping occurs, and RF radiation forces transitions between the Zeeman levels.

The change in the equilibrium population when switching from right-handed to left-handed circular pumped light is verified in the first experiment. The second and third experiments measure the Zeeman transitions in the ground state of the isotopes Rb-87 and Rb-85 and determine the nuclear spin I from the number of transitions observed. The observed transitions are classified through comparison with the Breit-Rabi formula. In the next two experiments, the measured transition frequencies are used for precise determination of the magnetic field B as a function of the magnet current I . The nuclear g factors g_I are derived using the measurement data. In the final experiment, two-quantum transitions are induced and observed for a high field strength of the irradiating RF field.

Cat. No.	Description	P 6.2.8.1	P 6.2.8.2-6
558 823	Rubidium high frequency lamp	1	1
558 826	Helmholtz coils on stand rider	1	1
558 833	Absorption chamber with rubidium absorption cell	1	1
558 835	Silicon photodetector	1	1
558 836	I/U-converter for silicon photodetector	1	1
530 88	Plug-in power unit, 9.2 V DC, regulated	1	1
558 814	Operational device for optical pumping	1	1
521 45	DC power supply 0...+/- 15 V	1	1
522 551	Function generator, 12 MHz, internal sweep		1
501 022	BNC cable, 2 m long		1
501 02	BNC cable, 1 m long	2	3
	Two channel/ XY storage oscilloscope, e.g. Analog/digital oscilloscope HM 507	1	1
531 281	Digital-analog multimeter METRAHit 24 S	1	1
504 48	Two-way switch	1	1
468 000	Line filter 795 nm	1	1
472 410	Polarization filter	1	1
472 611	Quarter-wavelength plate (200 nm)	1	1
460 021	Lens f = + 50 mm, brass handle	1	1
460 031	Lens f = + 100 mm, brass handle	1	1
460 32	Precision optical bench, standardized cross section, 1 m	1	1
460 370	Optics rider, H = 60 mm/W = 34 mm	6	6
460 374	Optics rider, H = 90 mm/W = 50 mm	1	1
666 768	Circulation thermostat 30 ... 100 °C	1	1
200 66843	Silicone tube, 1.0 m long, 6.0 x 2.0	2	2
501 28	Connecting lead, Ø 2.5 mm ² , 50 cm, black	4	4
501 38	Connecting lead, Ø 2.5 mm ² , 100 cm, black	2	2
666 7703	Pump set	1	1



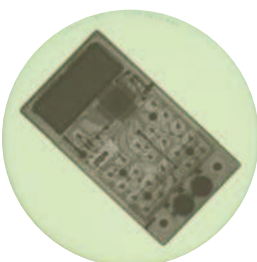
Determining the ion dose rate of the x-ray tube with molybdenum anode (P 6.3.1.4)

P 6.3.1**Detection of x-rays**

- P 6.3.1.1 Fluorescence of a luminescent screen due to x-rays
- P 6.3.1.2 X-ray photography: exposure of film stock due to x-rays
- P 6.3.1.3 Detecting x-rays using an ionization chamber
- P 6.3.1.4 Determining the ion dose rate of the x-ray tube with molybdenum anode

Cat. No.	Description	P 6.3.1.1	P 6.3.1.2	P 6.3.1.3-4
554 811USB	X-ray apparatus	1	1	1
554 838	X-ray film holder		1	
554 896	X-ray film Agfa Dentus M2		1	
554 897	Developer for X-ray film		1	
554 898	Fixative for X-ray film		1	
554 893	Development tank 500 ml		1*	
554 899	Changing bag for the development tank		1*	
554 840	Plate capacitor x-ray			1
522 27	Power supply 450 V DC		1	
532 14	Electrometer amplifier		1	
577 02	STE resistor 1 GΩ, 0.5 W		1	
	Voltmeter, DC, $U \leq 300$ V, e. g.			
531 120	Multimeter LD analog 20		1	
	Voltmeter, DC, $U \leq 10$ V, e. g.			
531 120	Multimeter LD analog 20		1	
575 24	Screened cable BNC/4 mm		1	
501 451	Pair of cables, 50 cm, black		1	
501 46	Pair of cables, 1 m, red and blue		1	
501 45	Pair of cables, 50 cm, red and blue		2	

* additionally recommended



Fluorescence of a luminescent screen due to x-rays (P 6.3.1.1)

Soon after the discovery of x-rays by *W. C. Röntgen*, physicians began to exploit the ability of this radiation to pass through matter which is opaque to ordinary light for medical purposes. The technique of causing a luminescent screen to fluoresce with x-ray radiation is still used today for screen examinations, although image amplifiers are used additionally. The exposure of a film due to x-ray radiation is used both for medical diagnosis and materials testing, and is the basis for dosimetry with films. As x-rays ionize gases, they can also be measured via the ionization current of an ionization chamber.

The first experiment demonstrates the transillumination with x-rays using simple objects made of materials with different absorption characteristics. A luminescent screen of zinc-cadmium sulfate is used to detect x-rays; the atoms in this compound are excited by the absorption of x-rays and emit light quanta in the visible light range. This experiment investigates the effect of the emission current I of the x-ray tube on the brightness and the effect of the high voltage U on the contrast of the luminescent screen.

The second experiment records the transillumination of objects using x-ray film. Measuring the exposure time required to produce a certain degree of exposure permits quantitative conclusions regarding the intensity of the x-rays.

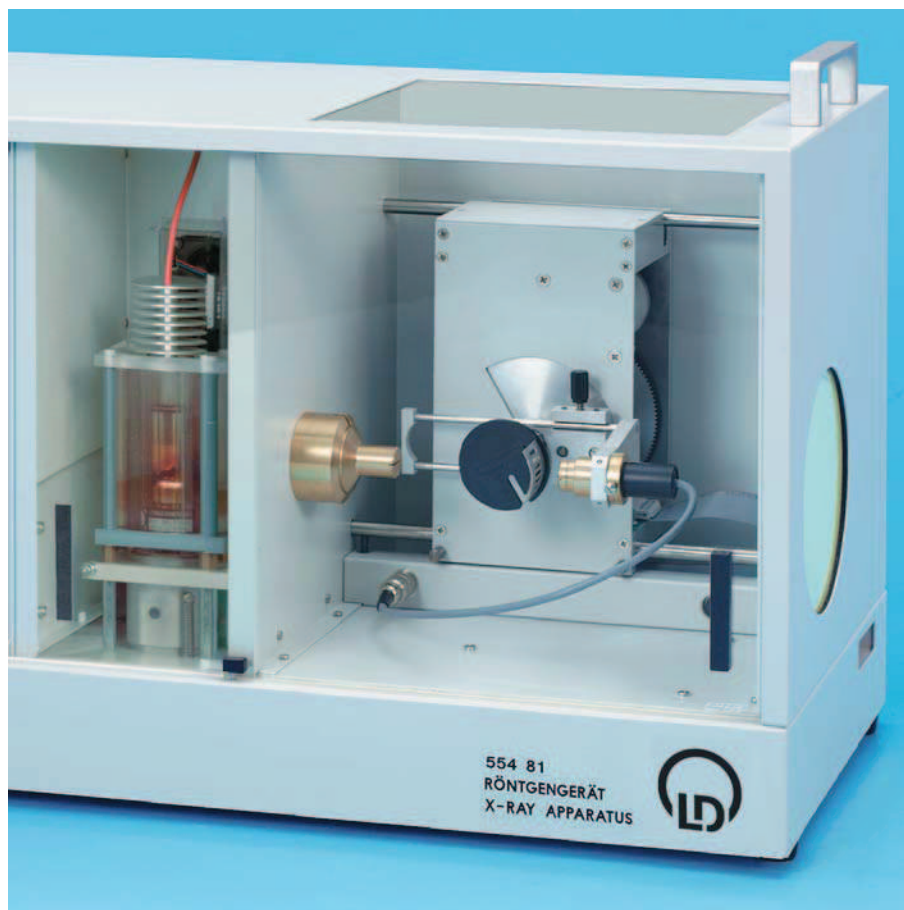
The aim of the last two experiments is to detect x-rays using an ionization chamber. First, the ionization current is recorded as a function of the voltage at the capacitor plates of the chamber and the saturation range of the characteristic curves is identified. Next, the mean ion dose rate

$$\bar{J} = \frac{I_{\text{ion}}}{m}$$

is calculated from the ionization current I_{ion} which the x-radiation generates in the irradiated volume of air V , and the mass m of the irradiated air. The measurements are conducted for various emission currents I and high voltages U of the x-ray tube.

P 6.3.2**Attenuation of x-rays**

- P 6.3.2.1 Investigating the attenuation of x-rays as a function of the absorber material and absorber thickness
- P 6.3.2.2 Investigating the wavelength dependency of the attenuation coefficient
- P 6.3.2.3 Investigating the relationship between the attenuation coefficient and the atomic number Z



Investigating the attenuation of x-rays as a function of the absorber material and absorber thickness (P 6.3.2.1)

The attenuation of x-rays on passing through an absorber with the thickness d is described by Lambert's law for attenuation:

$$I = I_0 \cdot e^{-\mu d}$$

I_0 : intensity of primary beam

I : transmitted intensity

Here, the attenuation is due to both absorption and scattering of the x-rays in the absorber. The linear attenuation coefficient μ depends on the material of the absorber and the wavelength λ of the x-rays. An absorption edge, i.e. an abrupt transition from an area of low absorption to one of high absorption, may be observed when the energy $h \cdot \nu$ of the x-ray quantum just exceeds the energy required to move an electron out of one of the inner electron shells of the absorber atoms.

The object of the first experiment is to confirm Lambert's law using aluminum and to determine the attenuation coefficients μ for six different absorber materials averaged over the entire spectrum of the x-ray apparatus.

The second experiment records the transmission curves

$$T(\lambda) = \frac{I(\lambda)}{I_0(\lambda)}$$

for various absorber materials. The aim of the evaluation is to confirm the λ^3 relationship of the attenuation coefficients for wavelengths outside of the absorption edges.

In the final experiment, the attenuation coefficient $\mu(\lambda)$ of different absorber materials is determined for a wavelength λ which lies outside of the absorption edge. This experiment reveals that the attenuation coefficient is closely proportional to the fourth power of the atomic number Z of the absorbers.

Cat. No.	Description	P 6.3.2.1	P 6.3.2.2	P 6.3.2.3
554 811USB	X-ray apparatus	1	1	1
559 01	End-window counter for α , β , γ - and x-rays	1	1	1
554 834	Absorption accessory x-ray	1		
554 832	Set of absorber foils		1	1
	additionally required:			
	1 PC with Windows 95/98/NT or higher		1	



Bragg reflection: diffraction of x-rays at a monocrystal (P 6.3.3.1)

P 6.3.3**Physics of the atomic shell**

- P 6.3.3.1 Bragg reflection: diffraction of x-rays at a monocrystal
- P 6.3.3.2 Investigating the energy spectrum of an x-ray tube as a function of the high voltage and the emission current
- P 6.3.3.3 Duane-Hunt relation and determination of Planck's constant
- P 6.3.3.4 Fine structure of the characteristic x-ray radiation of a molybdenum anode
- P 6.3.3.5 Edge absorption: filtering x-rays
- P 6.3.3.6 Moseley's law and determination of the Rydberg constant
- P 6.3.3.8 Fine structure of the characteristic x-ray radiation of a copper anode

Cat. No.	Description	P 6.3.3.1-5	P 6.3.3.6	P 6.3.3.8
554 811USB	X-ray apparatus	1	1	1
554 85	X-ray tube copper			1
559 01	End-window counter for α -, β -, γ - and x-rays	1	1	1
554 832	Set of absorber foils		1	
	additionally required: PC with Windows 95/98/NT or higher	1	1	1

The radiation of an x-ray tube consists of two components: continuous bremsstrahlung radiation is generated when fast electrons are decelerated in the anode. Characteristic radiation consisting of discrete lines is formed by electrons dropping to the inner shells of the atoms of the anode material from which electrons were liberated by collision.

To confirm the wave nature of x-rays, the first experiment investigates the diffraction of the characteristic K_α and K_β lines of the molybdenum anode at an NaCl monocrystal and explains these using Bragg's law of reflection.

The second experiment records the energy spectrum of the x-ray apparatus as a function of the high voltage and the emission current using a goniometer in the Bragg configuration. The aim is to investigate the spectral distribution of the continuum of bremsstrahlung radiation and the intensity of the characteristic lines.

The third experiment measures how the limit wavelength λ_{\min} of the continuum of bremsstrahlung radiation depends on the high voltage U of the x-ray tube. When we apply the Duane-Hunt relationship

$$e \cdot U = h \cdot \frac{c}{\lambda_{\min}}$$

e : electron charge,
 c : velocity of light

to the measurement data, we can derive Planck's constant h .

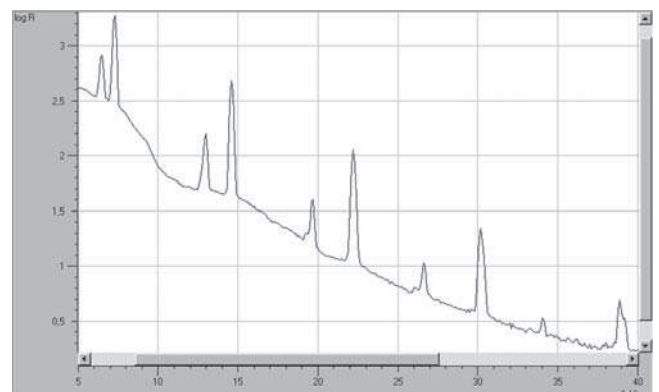
The fourth experiment reveals the fine structure of the characteristic lines K_α and K_β and explains these on the basis of the fine structure of the atomic levels involved.

The object of the fifth experiment is to filter x-rays using the absorption edge of an absorber, i.e. the abrupt transition from an area of low absorption to one of high absorption.

The sixth experiment determines the wavelengths λ_K of the absorption edges as a function of the atomic number Z . When we apply Moseley's law

$$\frac{1}{\lambda_K} = R \cdot (Z - \sigma)^2$$

to the measurement data we obtain the Rydberg constant R and the mean screening σ .

Splitting of the K_α and K_β -lines in the 3rd to 5th diffraction orders

P 6.3.5

X-ray energy spectroscopy

- P 6.3.5.1 Recording and calibrating an X-ray energy spectrum
- P 6.3.5.2 Recording the energy spectrum of a molybdenum anode
- P 6.3.5.3 Recording the energy spectrum of a copper anode
- P 6.3.5.4 Investigation of the characteristic spectra as a function of the element's atomic number: K-lines
- P 6.3.5.5 Investigation of the characteristic spectra as a function of the element's atomic number: L-lines
- P 6.3.5.6 Energy-resolved Bragg reflection in different orders of diffraction



Recording and calibrating an X-ray energy spectrum (P 6.3.5.1)

The X-ray energy detector enables recording of the energy spectrum of X-rays. The detector is a Peltier-cooled photodiode wherein the incoming X-rays produce electron-hole pairs. The number of electron-hole pairs and thus the voltage pulse height after amplification is proportional to the X-ray energy. The pulse height analysis is carried out with CASSY used as a multichannel analyzer (MCA-Box), which is connected to a computer (PC).

The object of the first experiment is to record the X-ray fluorescence spectrum of a target and to use the known energies for calibration of the energy axis. The target is made of a zinc-plated steel and emits several fluorescent lines.

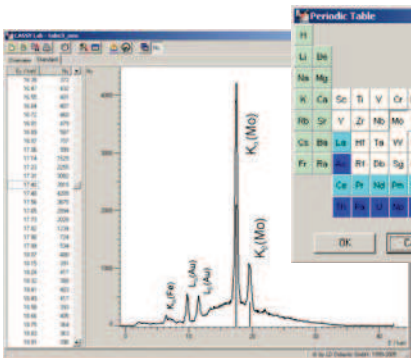
The second and third experiment use the calibrated detector to record emission spectra of either a molybdenum anode or a copper anode. The resulting spectrum shows the characteristic lines of the anode material and the bremsstrahlung continuum.

The fourth experiment demonstrates differences in the characteristic fluorescent K-lines (transitions to K-shell) within the X-ray spectra of different elements. These are used to confirm Moseley's law and show aspects of material analysis.

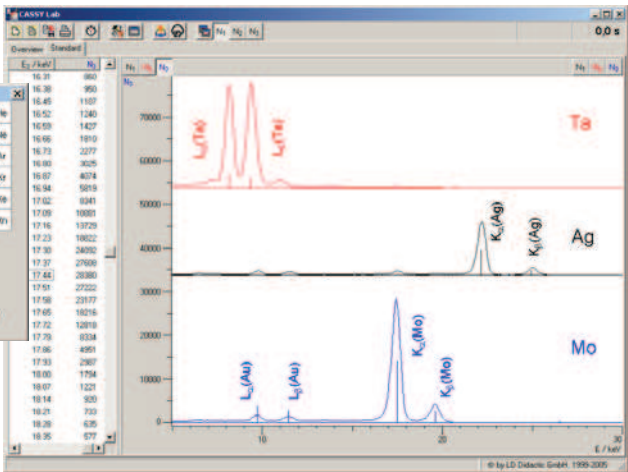
The fifth experiment shows similar characteristic fluorescent L-lines for heavier elements, demonstrating the X-ray emission from transitions to the L-shell.

Cat. No.	Description	P 6.3.5.1	P 6.3.5.2	P 6.3.5.3	P 6.3.5.4	P 6.3.5.5	P 6.3.5.6
554 811USB	X-ray apparatus	1	1	1	1	1	1
554 85	X-ray tube copper			1			1
559 938	X-ray energy detector	1	1	1	1	1	1
554 844	Set of targets K-line fluorescence				1		
554 846	Set of targets L-line fluorescence					1	
524 010USB	Sensor-CASSY	1	1	1	1	1	1
524 058	MCA Box	1	1	1	1	1	1
524 200	CASSY Lab	1	1	1	1	1	1
501 02	BNC Cable, 1 m	1	1	1	1	1	1
	additionally required: PC with Windows 98/NT or higher	1	1	1	1	1	1

In the sixth experiment using the X-ray energy detector in Bragg geometry it is possible to observe different X-ray energies simultaneously, because Bragg condition is fulfilled for different orders.



X-ray spectrum of molybdenum anode (P 6.3.5.2)



X-ray fluorescence of different elements. (P 6.3.5.4/5)



P 6.3.7**Compton effect on X-rays**

P 6.3.7.1 Compton effect: verifying the energy loss of the scattered X-ray quantum

P 6.3.7.2 Compton effect: Measurement of the energy of the scattered photons as a function of the scattering angle

Compton effect: Measurement of the energy of the scattered photons as a function of the scattering angle (P 6.3.7.2)

Cat. No.	Description	P 6.3.7.1	P 6.3.7.2
554 811USB	X-ray apparatus	1	1
559 01	End-window counter with cable	1	
554 836	Compton accessory X-ray	1	
554 837	Compton accessory X-ray II		1
559 938	X-ray energy detector		1
524 010USB	Sensor-CASSY		1
524 058	MCA Box		1
524 200	CASSY Lab		1
501 02	BNC Cable, 1 m		1
	additionally required: PC with Windows 98/NT or higher		1

At a time (early 1920's) when the particle nature of light (photons) suggested by the photoelectric effect was still being debated, the Compton experiment, the scattering of X-rays on weakly bound electrons, in 1923 gave another evidence of particle-like behaviour of X-rays in this process.

Compton investigated the scattering of X-rays passing through matter. According to classical physics the frequency of the radiation should not be changed by the scattering process. However, A. H. Compton observed a frequency change for scattered X-rays. He interpreted this in the particle model as a collision of the X-ray photon and an electron of the scattering material. Assuming total energy and momentum to be conserved, energy is transferred from the photon to the electron, so the energy of the scattered photon depends on the scattering angle ϑ .

The first experiment verifies the Compton shift using the end-window counter. The change of frequency or wavelength due to the scattering process is apparent as a change of the attenuation of an absorber, which is placed either in front of or behind the scattering body.

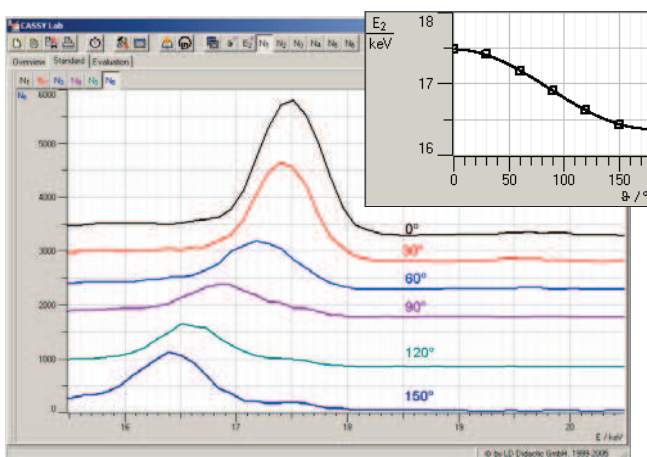
The object of the second experiment is to record directly the energy spectra of the scattered X-rays with the X-ray energy detector as a function of the scattering angle ϑ . The energy $E(\vartheta)$ of the scattered photons at different angles is determined and compared with the calculated energy obtained from conservation of energy and momentum by using the relativistic expression for the energy:

$$E(\vartheta) = \frac{E_0}{1 + \frac{E_0}{m \cdot c^2} \cdot (1 - \cos \vartheta)}$$

E_0 : energy of the photon before the collision

m : mass of electron at rest

c : velocity of light



Energy shift of the scattered X-rays at different angles (P 6.3.7.2)



Ionization of air due to radioactivity (P 6.4.1.1)

P 6.4.1**Detection of radioactivity**

- P 6.4.1.1 Ionization of air due to radioactivity
- P 6.4.1.2 Recording the current-voltage characteristic of an ionization chamber
- P 6.4.1.3 Detecting radioactivity using a Geiger counter
- P 6.4.1.4 Recording the characteristic of a Geiger-Müller counter tube

Cat. No.	Description	P 6.4.1.1	P 6.4.1.2	P 6.4.1.3	P 6.4.1.4
559 82	Am 241 preparation	1	1		
546 31	Zinc plate for photoelectric effect	1			
546 33	Grid electrode	1			
522 27	Power supply 450 V DC	1			
532 14	Electrometer amplifier	1			
532 16	Connection rod	1			1
577 03	STE resistor 10 GΩ, 0.5 W	1			
531 120	Voltmeter, DC, $U \leq 10$ V, e.g. Multimeter LD analog 20	1	1		
546 25	Ionization chamber		1		
521 70	High voltage power supply 10 kV		1	1	
532 00	I-measuring amplifier D		1		
575 24	Screened cable BNC/4 mm		1	1	
501 644	Set of 6 two-way plug adapters, black		1		
300 02	Stand base, V-shape, 20 cm		1		
300 41	Stand rod, 25 cm		1	1	
301 01	Leybold multiclamp		1	1	
666 555	Universal clamp, 0...80 mm dia.		1	1	
559 430	Ra 226 preparation			1	1
546 281	Geiger counter			1	
546 38	Adapter for geiger counter			1	
575 211	Two channel oscilloscope 303			1	
300 11	Saddle base			1	2
559 01	End-window counter for α , β , γ and x-rays				1
575 48	Digital counter				1
590 13	Insulated stand rod, 25 cm long			1	
591 21	Large clip plug				1
500 412	Connection lead, 25 cm, blue	1			
500 421	Connection lead, 50 cm, red		1		

In 1895, *H. Becquerel* discovered radioactivity while investigating uranium salts. He found that these emitted a radiation which was capable of fogging light-sensitive photographic plates even through black paper. He also discovered that this radiation ionizes air and that it can be identified by this ionizing effect.

In the first experiment, a voltage is applied between two electrodes, and the air between the two electrodes is ionized by radioactivity. The ions created in this way cause a charge transport which can be detected using an electrometer as a highly sensitive ammeter.

The aim of the second experiment is to record the current-voltage characteristic of air ionized by radioactivity in an ionization chamber. This experiment shows that, at low voltages, the current rises in proportion to the voltage. At higher voltages, the current reaches a saturation value, which depends on the intensity of the preparation.

The third experiment uses a Geiger counter to detect radioactivity. A potential is applied between a cover with hole which serves as the cathode and a fine needle as the anode; this potential is just below the threshold of the disruptive field strength of the air. As a result, each ionizing particle which travels within this field initiates a discharge collision.

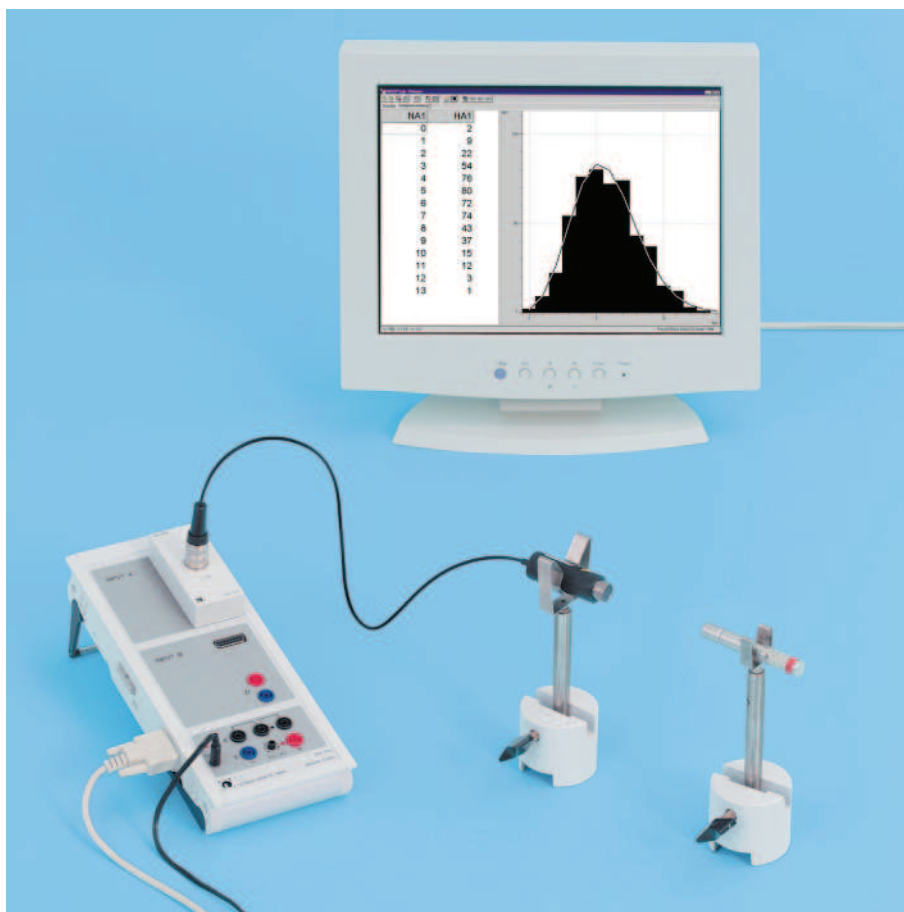
The final experiment records the current-voltage characteristic of a Geiger-Müller counter tube. Here too, the current increases proportionally to the voltage for low voltage values, before reaching a saturation value which depends on the intensity or distance of the preparation.

500 610	Safety connecting lead, 25 cm, yellow/green		1	1	
501 40	Connecting lead, \varnothing 2.5 mm ² , 25 cm, yellow/green		1		
501 45	Pair of cables, 50 cm, red and blue	2	1	1	
501 451	Pair of cables, 50 cm, black	1			

P 6.4.2

Poisson distribution

P 6.4.2.1 Statistical variations in
CASSY-5 determining counting rates



Statistical variations in determining counting rates (P 6.4.2.1)

For each individual particle in a radioactive preparation, it is a matter of coincidence whether it will decay over a given time period Δt . The probability that any particular particle will decay in this time period is extremely low. The number of particles n which will decay over time Δt thus shows a Poisson distribution around the mean value μ . In other words, the probability that n decays will occur over a given time period Δt is

$$w_{\mu}(n) = \frac{\mu^n}{n!} e^{-\mu}$$

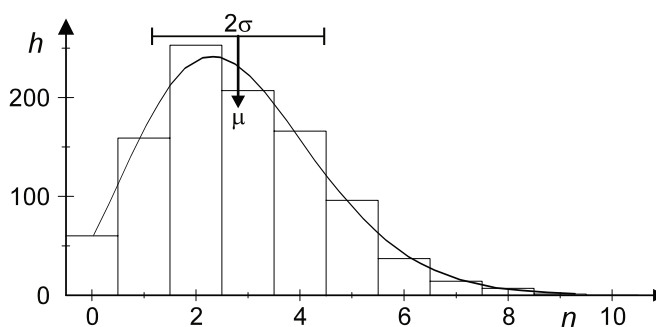
μ is proportional to the size of the preparation and the time Δt , and inversely proportional to the half-life $T_{1/2}$ of the radioactive decay.

Using a computer-assisted measuring system, this experiment determines multiple pulse counts n triggered in a Geiger-Müller counter tube by radioactive radiation over a selectable gate time Δt . After a total of N counting runs, the frequencies $h(n)$ are determined at which precisely n pulses were counted, and displayed as histograms. For comparison, the evaluation program calculates the mean value μ and the standard deviation

$$\sigma = \sqrt{\mu}$$

of the measured intensity distribution $h(n)$ as well as the Poisson distribution $w_{\mu}(N)$.

Cat. No.	Description	P 6.4.2.1
559 83	Set of 5 radioactive preparations	1
524 0331	Geiger-Müller counter tube S	1
524 010USB	Sensor-CASSY	1
524 200	CASSY Lab	1
591 21	Large clip plug	1
590 02	Small clip plug	1
532 16	Connection rod	2
300 11	Saddle base	2
	additionally required: PC with Windows 95/NT or higher	1



Measured and calculated Poisson distribution
 Histogram: $h(n)$, curve: $N \cdot w_{\mu}(n)$

**P 6.4.3****Radioactive decay and half-life**

P 6.4.3.3 Determining the half-life of Ba-137m – Point-by point recording of a decay curve

P 6.4.3.4 Determining the half-life of Ba-137m – recording and evaluating the decay curve using CASSY

Determining the half-life of Ba-137m – recording and evaluating the decay curve using CASSY (P 6.4.3.4)

Cat. No.	Description	P 6.4.3.3 (a)	P 6.4.3.3 (b)	P 6.4.3.4
559 815	Cs/Ba-137m isotope generator	1	1	1
559 01	End-window counter	1		
575 48	Digital counter	1		
524 010USB	Sensor-CASSY			1
524 200	CASSY Lab			1
524 0331	Geiger-Müller counter tube S		1	1
664 043	Test tubes, 160 x 16 diam.	1	1	1
664 103	Beaker, 250 ml, ss, hard glass	1	1	1
300 02	Stand base, V-shape, 20 cm	1	1	1
300 42	Stand rod, 47 cm	1	1	1
301 01	Leybold multiclamp	2	2	2
666 555	Universal clamp, 0 ... 80 mm dia.	2	2	2
	additionally required:			
	PC with Windows 95/NT or higher			1
524 009	Mobile-CASSY		1	

For the activity of a radioactive sample, we can say:

$$A(t) = \left| \frac{dN}{dt} \right|$$

Here, N is the number of radioactive nuclei at time t . It is not possible to predict when an individual atomic nucleus will decay. However, from the fact that all nuclei decay with the same probability, it follows that over the time interval dt , the number of radioactive nuclei will decrease by

$$dN = -\lambda \cdot N \cdot dt$$

λ : decay constant

Thus, for the number N , the law of radioactive decay applies:

$$N(t) = N_0 \cdot e^{-\lambda \cdot t}$$

N_0 : number of radioactive nuclei at time $t = 0$

Among other things, this law states that after the half-life

$$t_{1/2} = \frac{\ln 2}{\lambda}$$

the number of radioactive nuclei will be reduced by half.

To determine the half-life of Ba-137m, a plastic bottle with Cs-137 stored at salt is used. The metastable isotope Ba-137m arising from the β -decay is released by an elution solution. The half-time amounts to 2.6 minutes approx.

P 6.4.4

Attenuation of α , β and γ radiation

- P 6.4.4.1 Measuring the range of α radiation in air
- P 6.4.4.2 Attenuation of β radiation when passing through matter
- P 6.4.4.3 Confirming the law of distance for β radiation
- P 6.4.4.4 Absorption of γ radiation when passing through matter

Absorption of γ radiation when passing through matter (P 6.4.4.4)

High-energy α and β particles release only a part of their energy when they collide with an absorber atom. For this reason, many collisions are required to brake a particle completely. Its range R

$$R \propto \frac{E_0^2}{n \cdot Z}$$

depends on the initial energy E_0 , the number density n and the atomic number Z of the absorber atoms.

Low-energy α and β particles or γ radiation are braked to a certain fraction when passing through a specific absorber density dx , or are absorbed or scattered and thus disappear from the beam. As a result, the radiation intensity I decreases exponentially with the absorption distance x .

$$I = I_0 \cdot e^{-\mu \cdot x}$$

μ : attenuation coefficient

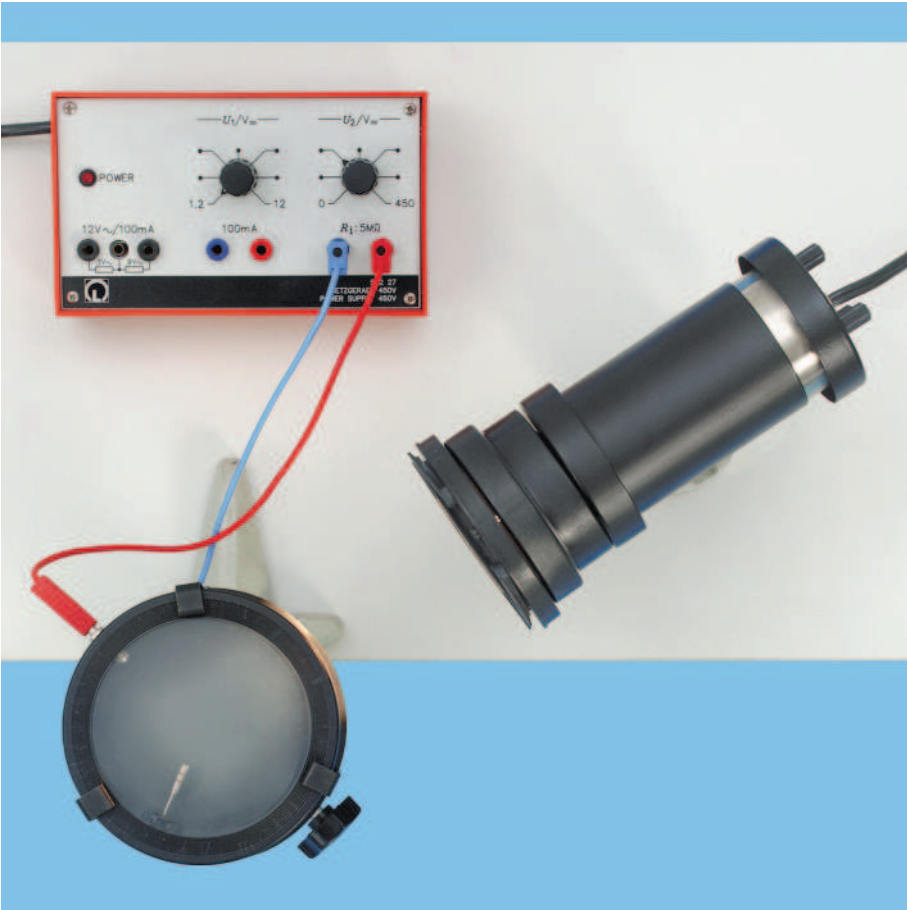
The first experiment determines the range R of monoenergetic α particles in air. Here, the ionization current I is measured in an ionization chamber of variable height as a function of the distance d between the cover and the Am-241 preparation. The ionization current initially increases with the distance d before remaining constant at distances which are greater than the range.

The second experiment examines the attenuation of β radiation from Sr-90 in aluminum as a function of the absorber thickness d . This experiment shows an exponential decrease in the intensity. As a comparison, the absorber is removed in the third experiment and the distance between the β preparation and the counter tube is varied. As one might expect for a point-shaped radiation source, the following is a good approximation for the intensity:

$$I(d) \propto \frac{1}{d^2}$$

The fourth experiment examines the attenuation of γ radiation in matter. Here too, the decrease in intensity is a close approximation of an exponential function. The attenuation coefficient μ depends on the absorber material and the γ energy.

Cat. No.	Description	P 6.4.4.1	P 6.4.4.2	P 6.4.4.3	P 6.4.4.4
559 82	Am 241 preparation	1			
546 25	Ionization chamber	1			
546 27	Telescopic cylinder	1			
546 35	Adapter for ionization chamber	1			
521 70	High voltage power supply 10 kV	1			
532 00	I-measuring amplifier D	1			
575 24	Screened BNC/4 mm	1			
531 120	Multimeter LDanalog 20	1			
311 53	Vernier calipers	1			
300 02	Stand base, V-shape, 20 cm	1			1
300 41	Stand rod, 25 cm	1			
301 01	Leybold multiclamp	1			3
666 555	Universal clamp, 0...80 mm dia.	1			1
500 610	Safety connecting lead, 25 cm, yellow/green	1			
501 40	Connecting lead, Ø 2.5 mm ² , 25 cm, yellow/green	1			
501 45	Pair of cables, 50 cm, red and blue	2			
559 83	Set of 5 radioactive preparations		1	1	1
559 18	Holder with absorber foils		1		
559 01	End-window counter for α , β , γ and x-rays		1	1	
575 471	Counter S		1	1	
590 02	Small clip plug		1	1	1
591 21	Large clip plug		1	1	
532 16	Connection rod		2	2	1
300 11	Saddle base		2	2	
460 97	Scaled metal rail, 0.5 m			1	
667 9182	Geiger counter				1
559 94	Set of absorbers and targets				1
666 572	Stand ring with stem, 7 cm dia.				1
300 42	Stand rod, 47 cm				1



P 6.5.1

Demonstration of particle tracks

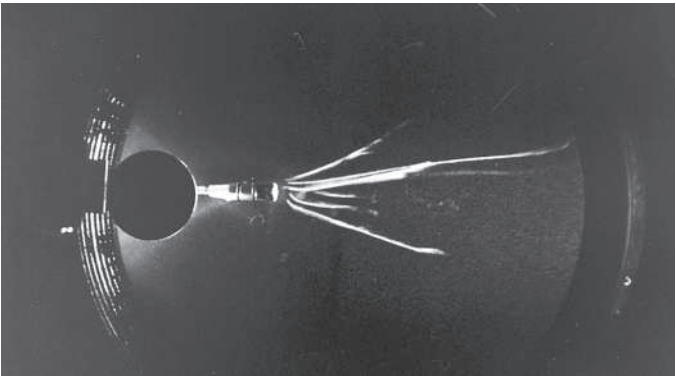
P 6.5.1.1 Demonstrating the tracks of α -particles in the Wilson cloud chamber

Demonstrating the tracks of α -particles in the Wilson cloud chamber (P 6.5.1.1)

Cat. No.	Description	P 6.5.1.1
559 57	Wilson cloud chamber	1
559 59	Radium source for Wilson cloud chamber	1
522 27	Power supply 450 V DC	1
450 60	Lamp housing	1
450 51	Lamp, 6 V/30 W	1
460 20	Aspherical condensor	1
521 210	Transformer, 6 V AC,12 V AC/30 VA	1
301 06	Bench clamp	1
300 11	Saddle base	1
671 9720	Ethanol, fully denaturated, 1l	1
501 46	Pair of cables, 1 m, red and blue	1

In a Wilson cloud chamber, a saturated mixture of air, water and alcohol vapor is briefly caused to assume a supersaturated state due to adiabatic expansion. The supersaturated vapor condenses rapidly around condensation seeds to form tiny mist droplets. Ions, which are formed e.g. through collisions of α particles and gas molecules in the cloud chamber, make particularly efficient condensations seeds.

In this experiment, the tracks of α particles are observed in a Wilson cloud chamber. Each time the pump is vigorously pressed, these tracks are visible as traces of droplets in oblique light for one to two seconds. An electric field in the chamber clears the space of residual ions.



Droplet traces in the Wilson cloud chamber

P 6.5.2

Rutherford scattering

P 6.5.2.1 Rutherford scattering:
measuring the scattering rate
as a function of the scattering
angle and the atomic number

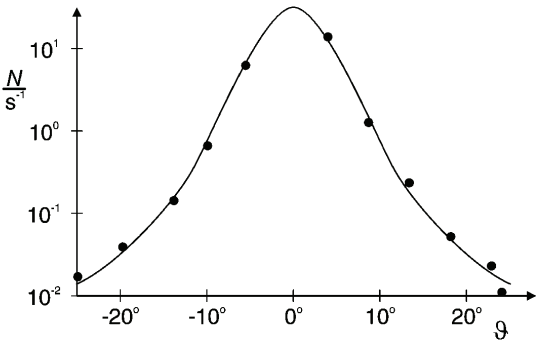


Rutherford scattering: measuring the scattering rate as a function of the scattering angle and the atomic number (P 6.5.2.1)

The fact that an atom is “mostly empty space” was confirmed by *Rutherford, Geiger* and *Marsden* in one of the most significant experiments in the history of physics. They caused a parallel beam of α particles to fall on an extremely thin sheet of gold leaf. They discovered that most of the α particles passed through the gold leaf virtually without deflection, and that only a few were deflected to a greater degree. From this, they concluded that atoms consist of a virtually massless extended shell, and a practically point-shaped massive nucleus.

This experiment reproduces these observations using an Am-241 preparation in a vacuum chamber. The scattering rate $N(\vartheta)$ is measured as a function of the scattering angle ϑ using a Geiger-Müller counter tube. As scattering materials, a sheet of gold leaf ($Z = 80$) and aluminum foil ($Z = 13$) are provided. The scattering rate confirms the relationship

$$N(\vartheta) \propto \frac{1}{\sin^4 \frac{\vartheta}{2}} \text{ and } N(\vartheta) \propto Z^2.$$



Scattering rate N as a function of the scattering angle ϑ

Cat. No.	Description	P 6.5.2.1	
559 82	Am 241 preparation	1	
559 56	Rutherford scattering chamber	1	
559 52	Aluminum foil in holder	1	
559 931	Discriminator preamplifier	1	
562 791	Plug-in power unit	1	
575 471	Counter S	1	
378 73	Rotary-vane vacuum pump S 1.5	1	
378 031	Small flange DN 16 KF with hose nozzle	1	
667 186	Vacuum tubing, 8/18 mm dia.	1	
501 01	BNC cable, 25 cm long	1	
575 24	Screened cable BNC/4 mm	1	





P 6.5.3

Nuclear magnetic resonance (NMR)

P 6.5.3.1 Nuclear magnetic resonance in polystyrene, glycerine and Teflon

Nuclear magnetic resonance in polystyrene, glycerine and Teflon (P 6.5.3.1 a)

Cat. No.	Description	P 6.5.3.1 (a)	P 6.5.3.1 (b)
514 602	NMR supply unit	1	1
514 606	NMR probe unit	1	1
562 11	U-core with yoke	1	1
562 131	Coil, 10 A, 480 turns	2	2
521 545	DC power supply 0...16 V, 5 A	1	1
575 294	Analog/digital oscilloscope HM 507	1	
501 02	BNC cable, 1 m long	2	
531 835	Universal Measuring Instrument Physics	1*	
524 0381	Combi B-Sensor S	1*	
501 11	Extension cable, 15-pole	1*	
524 010USB	Sensor-CASSY		1
524 200	CASSY Lab		1
575 24	Screened cable BNC/4 mm		2
500 621	Safety connection lead, 50 cm, red	1	1
500 641	Safety connection lead, 100 cm, red	1	1
500 642	Safety connection lead, 100 cm, blue	1	1
	additionally required: PC with Windows 95/98/NT or higher		1

* additionally recommended

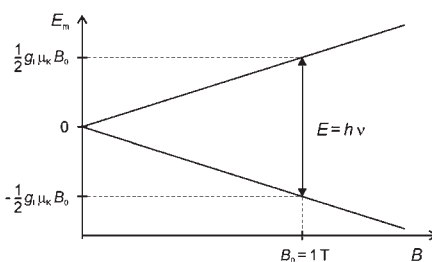


Diagram of resonance condition of hydrogen

The magnetic moment of the nucleus entailed by the nuclear spin / assumes the energy states

$$E_m = -g_l \cdot \mu_K \cdot m \cdot B \text{ with } m = -l, -l+1, \dots, l$$

$$\mu_K = 5,051 \cdot 10^{-27} \frac{\text{J}}{\text{T}}: \text{ nuclear magneton}$$

g_l : g factor of nucleus

in a magnetic field B . When a high-frequency magnetic field with the frequency ν is applied perpendicularly to the first magnetic field, it excites transitions between the adjacent energy states when these fulfill the resonance condition

$$h \cdot \nu = E_{m+1} - E_m$$

h : Planck's constant

This fact is the basis for nuclear magnetic resonance, in which the resonance signal is detected using radio-frequency technology. For example, in a hydrogen nucleus the resonance frequency in a magnetic field of 1 T is about 42.5 MHz. The precise value depends on the chemical environment of the hydrogen atom, as in addition to the external magnetic field B the local internal field generated by atoms and nuclei in the near vicinity also acts on the hydrogen nucleus. The width of the resonance signal also depends on the structure of the substance under study.

This experiment verifies nuclear magnetic resonance in polystyrene, glycerine and Teflon. The evaluation focuses on the position, width and intensity of the resonance lines.

P 6.5.4 **α spectroscopy**

P 6.5.4.1 α spectroscopy of radioactive samples
CASSY-S

P 6.5.4.2 Determining the energy loss of α radiation in air
CASSY-S

P 6.5.4.3 Determining the energy loss of α radiation in aluminum and in gold
CASSY-S

P 6.5.4.4 Determining the age of an Ra-226 sample
CASSY-S



α spectroscopy of radioactive samples (P 6.5.4.1)

Up until about 1930, the energy of α rays was characterized in terms of their range in air. For example, a particle of 5.3 MeV (Po-210) has a range of 3.84 cm. Today, α energy spectra can be studied more precisely using semiconductor detectors. These detect discrete lines which correspond to the discrete excitation levels of the emitting nuclei.

The aim of the first experiment is to record and compare the α energy spectra of the two standard preparations Am-241 and Ra-226. To improve the measuring accuracy, the measurement is conducted in a vacuum chamber.

In the second experiment, the energy E of α particles is measured as a function of the air pressure p in the vacuum chamber. The measurement data is used to determine the energy per unit of distance dE/dx which the α particles lose in the air. Here,

$$x = \frac{p}{p_0} \cdot x_0$$

x_0 : actual distance, p_0 : standard pressure

is the apparent distance between the preparation and the detector.

The third experiment determines the amount of energy of α particles lost per unit of distance in gold and aluminum as the quotient of the change in the energy ΔE and the thickness Δx of the metal foils.

In the final experiment, the individual values of the decay chain of Ra-226 leading to the α energy spectrum are analyzed to determine the age of the Ra-226 preparation used here. The activities A_1 and A_2 of the decay chain "preceding" and "following" the longer-life isotope Pb-210 are used to determine the age of the sample from the relationship

$$A_2 = A_1 \cdot \left(1 - e^{-\frac{T}{\tau}}\right)$$

$\tau = 22.3 \text{ a}$: lifetime of Pb-210

Cat. No.	Description	P 6.5.4.1	P 6.5.4.2	P 6.5.4.3	P 6.5.4.4
559 82	Am 241 preparation	1	1	1	
559 430	Ra 226 preparation	1		1	1
559 56	Rutherford scattering chamber	1	1	1	1
559 52	Aluminium foil in holder			1	
559 931	Discriminator preamplifier	1	1	1	1
524 010USB	Sensor-CASSY	1	1	1	1
524 058	MCA Box	1	1	1	1
524 200	CASSY Lab	1	1	1	1
501 16	Multicore cable, 6-pole, 1.5 m	1	1	1	1
501 02	BNC cable, 1 m	1	1	1	1
501 01	BNC cable, 0.25 m	1	1	1	1
575 211	Two-channel oscilloscope 303	1*			
378 73	Rotary-vane vacuum pump S 1.5	1	1	1	1
667 186	Vacuum tubing 8/18 mm	1	1	1	1
378 031	Small flange DN 16 KF with hose nozzle	1	1	1	1
378 045	Centering ring DN 16 KF		4		
378 050	Clamping ring DN 10/16 KF		4		
378 015	Cross DN 16 KF		1		
378 776	Metering valve DN 16 KF		1		
378 510	Pointer manometer			1	
additionally required:					
1 PC with Windows 95/NT or higher		1	1	1	1

* additionally recommended

Absorption of γ radiation (P 6.5.5.3)**P 6.5.5** **γ spectroscopy**

P 6.5.5.1 Detecting γ radiation with a scintillation counter
CASSY-S

P 6.5.5.2 Recording and calibrating a γ spectrum
CASSY-S

P 6.5.5.3 Absorption of γ radiation
CASSY-S

P 6.5.5.4 Identifying and determining the activity of weakly radioactive samples
CASSY-S

P 6.5.5.5 Recording a β spectrum using a scintillation counter
CASSY-S

P 6.5.5.6 Coincidence and γ - γ angular correlation in positron decay
CASSY-S

Cat. No.	Description	P 6.5.5.1	P 6.5.5.2	P 6.5.5.3	P 6.5.5.4	P 6.5.5.5	P 6.5.5.6
559 84	Mixed preparation α , β , γ	1					
559 83	Set of 5 radioactive preparations		1	1		1	1
559 885	Calibrating preparation ^{137}Cs , 5 kBq				1		
559 901	Scintillation counter	1	1	1	1	1	2
559 912	Detector-output stage	1	1	1	1	1	2
559 94	Set of absorbers and targets			1		1	
559 89	Scintillator screening				1	1	
559 891	Socket for scintillator	1	1	1	1	1	1
559 88	Marinelli beaker				2		
521 68	High voltage power supply 1.5 kV	1	1	1	1	1	2
524 010USB	Sensor-CASSY	1	1	1	1	1	1
524 058	MCA Box	1	1	1	1	1	2
524 200	CASSY Lab	1	1	1	1	1	1
575 211	Two-channel oscilloscope 303	1*					
501 02	BNC cable, 1 m	1*					
300 42	Stand rod, 47 cm	1	1	1		1	1
301 01	Leybold multiclamp	1	1	1		1	1
666 555	Universal clamp, 0...80 mm dia.	1	1	1		1	1
672 5210	Potassium chloride, 250 g				4		
	additionally required: PC with Windows 95/NT or higher	1	1	1	1	1	1

* additionally recommended

When interpreting γ energy spectra recorded with a scintillation counter, it is necessary to take several interactive processes of the γ radiation with the scintillator crystal into consideration. In the photoeffect, the γ quanta transfer their entire energy to the crystal and are registered in the total absorption peak. Due to

Compton scattering, it often occurs that only a part of the γ energy is transferred to the crystal, as there is a certain probability that the scattered γ quantum will exit the crystal. The γ quanta are registered in a continuous distribution in which the upper and lower limits are determined by the maximum and minimum energy which can be transferred to the electron in Compton scattering. A third possible interaction, pair formation, is only significant at γ energies above 2 MeV.

In the first experiment, the output pulses of the scintillation counter are investigated using the oscilloscope and the multi-channel analyzer MCA-CASSY. The total absorption peak and the Compton distribution are identified in the pulse-amplitude distribution generated with monoenergetic γ radiation.

The aim of the second experiment is to record and compare the γ energy spectra of standard preparations. The total absorption peaks are used to calibrate the energy of the scintillation counter and to identify the preparations.

The third experiment examines the attenuation of γ radiation in various absorbers. The aim here is to show how the attenuation coefficient μ depends on the absorber material and the γ energy.

A Marinelli beaker is used in the fourth experiment for quantitative measurements of weakly radioactive samples. This apparatus encloses the scintillator crystal virtually completely, ensuring a defined measurement geometry. Lead shielding considerably reduces the interfering background from the laboratory environment.

The final experiment records the continuous spectrum of a pure β radiator ($^{90}\text{Sr}/^{90}\text{Y}$) using the scintillation counter. To determine the energy loss dE/dx of the β particles in aluminum, aluminum absorbers of various thicknesses x are placed in the beam path between the preparation and the detector.

P 6.5.6

Compton effect

P 6.5.6.1 Quantitative observation of the Compton effect
CASSY-S



Quantitative observation of the Compton effect (P 6.5.6.1)

In the Compton effect, a photon transfers a part of its energy E_0 and its linear momentum

$$p_0 = \frac{E_0}{c}$$

c : speed of light in a vacuum

to a free electron by means of elastic collision. Here, the laws of conservation of energy and momentum apply just as for the collision of two bodies in mechanics. The energy

$$E(\vartheta) = \frac{E_0}{1 + \frac{E_0}{m \cdot c^2} \cdot (1 - \cos \vartheta)}$$

m : mass of electron at rest

and the linear momentum

$$p = \frac{E}{c}$$

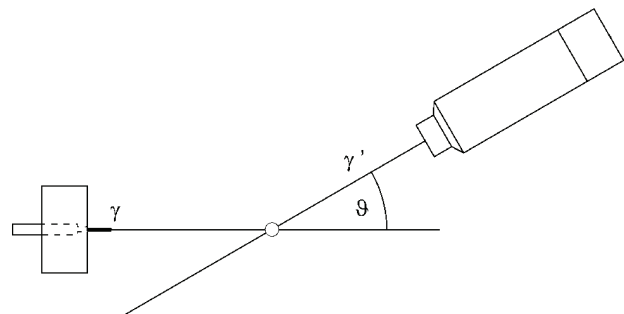
of the scattered photon depend on the scattering angle ϑ . The effective cross-section depends on the scattering angle and is described by the *Klein-Nishina* formula:

$$\frac{d\sigma}{d\Omega} = \frac{1}{2} \cdot r_0^2 \cdot \frac{p^2}{p_0^2} \cdot \left(\frac{p_0}{p} + \frac{p}{p_0} - \sin^2 \vartheta \right)$$

$r_0 = 2,5 \cdot 10^{-15}$ m: classic electron radius

In this experiment, the Compton scattering of γ quanta with the energy $E_0 = 667$ keV at the quasi-free electrons of an aluminum scattering body is investigated. For each scattering angle ϑ , a calibrated scintillation counter records one γ spectrum with and one without aluminum scatterer as a function of the respective scattering angle. The further evaluation utilizes the total absorption peak of the differential spectrum. The position of this peak gives us the energy $E(\vartheta)$. Its integral counting rate $N(\vartheta)$ is compared with the calculated effective cross-section.

Cat. No.	Description	P 6.5.6.1
559 800	Apparatus set Compton	1
559 809	Cs-137 preparation, 3.7 MBq	1
559 84	Mixed preparation alpha, beta, gamma	1
559 901	Scintillation counter	1
559 912	Detector output stage	1
521 68	High voltage power supply 1.5 kV	1
524 010USB	Sensor-CASSY	1
524 058	MCA Box	1
524 200	CASSY Lab	1
	additionally required:	
	PC with Windows 95/NT or higher	1



Measuring arrangement